



Review

Progress of Near-Infrared-Based Medical Imaging and Cancer Cell Suppressors

Vicky Mudeng^{1,2} , Gelan Ayana¹ , Sung-Uk Zhang^{3,*} and Se-woon Choe^{1,4,*}

¹ Department of Medical IT Convergence Engineering, Kumoh National Institute of Technology, Gumi 39253, Korea

² Department of Electrical Engineering, Institut Teknologi Kalimantan, Balikpapan 76127, Indonesia

³ Digital Twin Lab., Department of Automotive Engineering, Dong-Eui University, Busan 47340, Korea

⁴ Department of IT Convergence Engineering, Kumoh National Institute of Technology, Gumi 39253, Korea

* Correspondence: zsunguk@deu.ac.kr (S.-U.Z.); sewoon@kumoh.ac.kr (S.-w.C.)

Abstract: Diffuse optical tomography, an imaging modality that utilizes near-infrared light, is a new way to assess soft tissue. It provides a non-invasive screening of soft tissue, such as the breast in females and prostate in males, to inspect the existence of cancer. This new imaging method is considered cost-effective and preferred because the implementation is simply through the application of a laser or light-emitting diode as a light source. Near-infrared technology does not only offer cancer screening modality, but also acts as a cancer treatment method, called near-infrared photodynamic therapy. Despite plentiful studies in the area of near-infrared technology for cancer imaging and cancer cell suppression, there is no consolidated review that provides an overview of near-infrared application in cancer cell imaging and therapy. The objective of this study is to review near-infrared-based medical imaging and novel approaches to eradicate cancer cells. Additionally, we have discussed prospective instrumentation to establish cancer therapeutics apparatuses based on near-infrared technology. This review is expected to guide researchers implementing near-infrared for a medical imaging modality and cancer suppression in vitro, in vivo, and in clinical settings.



Citation: Mudeng, V.; Ayana, G.; Zhang, S.-U.; Choe, S.-w. Progress of Near-Infrared-Based Medical Imaging and Cancer Cell Suppressors. *Chemosensors* **2022**, *10*, 471. <https://doi.org/10.3390/chemosensors10110471>

Academic Editor: Antonio Fernandez

Received: 9 October 2022

Accepted: 8 November 2022

Published: 11 November 2022

Publisher's Note: MDPI stays neutral with regard to jurisdictional claims in published maps and institutional affiliations.



Copyright: © 2022 by the authors. Licensee MDPI, Basel, Switzerland. This article is an open access article distributed under the terms and conditions of the Creative Commons Attribution (CC BY) license (<https://creativecommons.org/licenses/by/4.0/>).

Keywords: near-infrared; diffuse optical tomography; imaging modality; cancer treatment; photodynamic therapy

1. Introduction

The electromagnetic spectrum is composed of a range of wavelengths categorized as low (gamma, X-rays, ultraviolet), middle (visible light that can be seen with the naked eye), and high (infrared, microwaves, radio) [1]. The infrared range of spectra can be further broken down into near-infrared, middle infrared, and far-infrared [2]. Near-infrared (NIR) is a type of light outside our visible spectrum of light [3]. It has wavelengths that are the closest to visible light, ranging 800–2500 nm. It is commonly used in light therapy for its natural healing benefits [4]. Health applications of NIR light generally use wavelengths of 810, 850, or 980 nm [5]. The application of NIR in cancer can be broadly categorized into imaging and therapeutic applications.

Near-infrared has elucidated promise in the biological imaging field. Compared to the visible optical region with 400–700 nm of the spectral windows, NIR spectral windows penetrate biological components, such as blood and skin. NIR provides various advantages, for instance, higher resolution and deeper propagation along with fewer optical properties (absorption and scattering coefficients) [6]. Additionally, it offers non-invasive and non-ionization properties, providing non-harmful medical procedures in a clinical setting [7]. Such merits initiated the use of NIR as an imaging modality to detect the presence of tumors inside soft tissue, such as the breast and prostate, as well as for screening the skull and thyroid gland [8–10]. NIR implementation as an imaging modality is known as diffuse optical imaging (DOI) or diffuse optical tomography (DOT) [11]. The ability of the

NIR-DOT imaging depends on several factors, such as the number of sensor pairs, source type, wavelength, and source and detector fabrication. Despite DOT based on NIR's use of simple instrumentation to visualize soft tissue, the imaging proficiency may decrease in the terms of sensitivity, contrast, and resolution due to the light excitation attenuation [12]. Moreover, light absorption and scattering are affected by the blood circulation and other biological mechanisms when it penetrates the body [13]. These conditions may create unnecessary artifacts in the background of the reconstructed images [10,14–16]. Regardless of its limitations, NIR-DOT has demonstrated its feasibility in cancer tissue evaluation. A common spectral window of NIR is 800–900 nm and is known as NIR-I [17,18]. Such windows were popular until NIR-II was identified several years ago, which has 1000–1700 nm of wavelength, and attracts significant attention in imaging technique research direction to overcome the NIR-I deficiencies [19,20]. NIR-II can offer minimal biological moieties; hence, it may enhance the spatial resolution, sensitivity, imaging fidelity, and deeper light propagation affecting the reduction in the unwanted background area [21].

The second application of NIR is a cancer therapy, known as NIR photodynamic therapy (NIR-PDT). NIR-PDT is praised because it can eradicate cancer with highly selective area treatment [17,22]. NIR-PDT is a newly developed and highly selective cancer treatment that induces an antibody–photoabsorber conjugate (AbPC) blended with NIR light [23,24]. The procedure injects the AbPC into the patient, which binds to the tumor within 24 h. The NIR radiation exposes the tumor by activating the conjugate, causing a photochemical reaction that selectively exterminates the cancer cells. Clinical trials targeting the epidermal growth factor receptor (EGFR) for recurrent head/neck cancer have shown effective treatment [25,26]. NIR-PDT helps cancer patients by preventing the side effects of surgery, radiation, and chemotherapy [27–29]. NIR therapy offers the advantages of boosting metabolism, recharging mitochondria, stimulating white blood cell production, reducing body fat, promoting cell regeneration, increasing energy, reducing inflammation within the body, improving circulation within the body, healing wounds faster, and others [30–33].

Despite its advantages, NIR applications for cancer imaging and treatment have limitations [34,35]. NIR has low penetration depth leading to increased sensitivity to superficial layers of tissue [2]. Sometimes, it is difficult to separate absorption and scattering [19]. Furthermore, NIR suffers from a low sampling rate resulting in a greater loss of photons [5]. Finally, the instrumentation has the disadvantages of being of larger weight, requiring a cooling or stabilization system, and being susceptible to noise [6]. To address these challenges, a few studies focusing on improving NIR application for cancer imaging and therapy have been performed. However, it is hard to find an organized document carefully analyzing the trends, challenges, and future directions of NIR applications in cancer imaging and therapy. According to the two aforementioned most popular applications of NIR for cancer, this paper attempts to review the NIR studies related to cancer imaging and treatment applications. Moreover, this review provides an additional contribution for NIR for cancer research by offering a simple instrumentation design to establish an NIR system for cancer treatment, including illustration of the prospective instruments by integrating the NIR-I and NIR-II wavelengths, single and multi-frequency DOT, and the combined techniques between visible, NIR, and other modalities, such as ultrasound, as well as continuous-wave (CW), frequency-domain (FD), and time-domain (TD) light sources.

2. NIR Instrumentation and Its Role in Cancer Diagnosis and Treatment

A computer, a fiber-optic accessory with NIR-radiation lighting and detecting fibers, and an NIR spectrometer make up the conventional NIR measuring instrumentation [8]. Radiation-emitting fibers carry the radiation from a broad-band, thermal, light-emitting diode or laser source to the tissue [13]. The chromophores in the target tissue (water, different types of hemoglobin, cytochromes, lipids, proteins, and deoxy-ribonucleic acid (DNA)) absorb the emitted radiation at particular wavelengths [36]. The photons that are transmitted or reflected back from the tissue are then gathered by the detecting fibers and

sent to the spectrometer for analysis. For diagnosis, a plot of the attenuation of radiation due to tissue scattering and absorption at each wavelength is created [13].

The therapeutic environment has seen a significant change in the previous ten years due to enhanced cancer immunotherapies [23]. However, changing the delicate balance between effector T cells and immunological suppressor cells is necessary for immunotherapy to be effective. Even though immunotherapy has the potential to yield amazing results, its overall response rate is still quite low, largely due to tumors' lack of T-cell penetration. Immune-related adverse events (irAEs), which are side effects of immunotherapy, have been extensively documented and frequently mirror autoimmune disease [37]. Two prevalent checkpoint inhibitors, anticytotoxic T-lymphocyte antigen-4 (CTLA-4) drugs and programmed death-1 (PD-1)/PD-ligand 1 (PD-L1) inhibitors, have been shown to cause immune-related adverse events (irAEs) in up to 90% of patients who received them [23]. Therefore, despite advancements, no cancer treatment is able to kill cancer cells just by triggering the immune response of the host in the area. To address these issues, near-infrared photoimmunotherapy is suggested.

3. Diffuse Optical Tomography

3.1. Forward Problem and Inverse Solution

DOT is an implementation of NIR as the imaging modality. NIR-DOT has become popular in the last decade because it offers simple tissue screening with an adequate reconstruction result. The light of NIR-DOT can penetrate the tissue; hence, when it infiltrates the tissue, some of the light will be absorbed and others are scattered due to the tissue optical properties. In the NIR-DOT mechanism, there are two optical properties, namely absorption μ_a and reduced scattering μ'_s coefficients [14,35,38]. A fundamental principle of NIR-DOT measurement is employed as a forward problem (to solve the diffusion equation (DE), which is the derivative model from a radiative transport equation (RTE)) and an inverse solution (to predict the map of optical properties to locate the tumor inside the soft tissue) [39,40].

Figure 1 depicts the illustration of the NIR-DOT measurement process. Several light sources (red rectangle) and detectors (green triangle) (source detector (SD)) are placed on the tissue (yellow circle) boundary. The number of SD can be adjusted according to the designed task under the test. For instance, Chen et al. [41] designed the NIR-DOT system with 16×16 of SD; thus, it had 256 measurements of light intensity and phase difference, whereas in a more advanced environment, in 2019, Cochran et al. [42] developed their NIR-DOT incorporating the combined evaluation of CW and TD. Similarly, their developed system was the integration approach between DOT and magnetic resonance imaging (MRI). Their DOT-MRI structure utilized five source lights for CW with different wavelengths of 670, 785, 808, 850, and 915 nm, while the TD measurement was with six laser sources at 650, 750, 780, 798, 838, and 905 nm wavelengths. They assigned charge-coupled device (CCD) cameras with fibers at the 108-degree position to detect the light intensity for CW measure, while photomultiplier tubes (PMTs) were located at the 8-degree position for TD measurement.

Inside the tissue, as shown in Figure 1, a defect (magenta circle) is presented to mimic a tumor in the biological tissue. When light from the sources, illustrated by the dark arrows, propagates through the tissue, some of the light is absorbed by the tissue and the defect, while some of the light is scattered deeper inside the tissue until it can invade the defect. The tissue and defect have their own optical properties; hence, the differences of μ_a and μ'_s generate light attenuation between the tissue and defect. This state produces a mapping of contrast in optical properties when the reconstructed images are obtained. Moreover, 1 is the light penetrating inside the tissue, 2 is the light penetrating back to the detector, and 3 is the light penetrating through the defect.

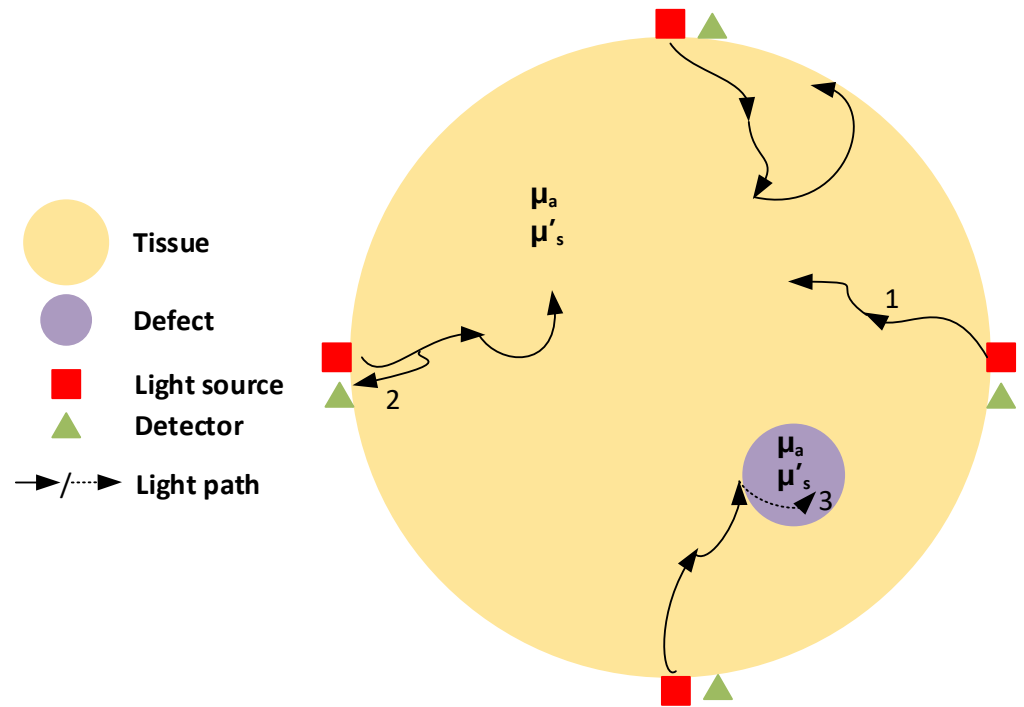


Figure 1. NIR-DOT measurement demonstration. The yellow circle is tissue, the magenta circle is a defect, the red rectangle is the light source, the green triangle is the detector, and the dark arrow is the light path. Additionally, 1 is the light penetrating inside the tissue, 2 is the light penetrating back to the detector, and 3 is the light penetrating through the defect.

The entire process of NIR-DOT can be stated by the differential equation (DE) in the forward problem, as below.

$$\nabla \cdot D(\mathbf{r}) \nabla \phi(\mathbf{r}, \omega) - \left[\mu_a(\mathbf{r}) - \frac{i\omega}{c} \right] \phi(\mathbf{r}, \omega) = -S_0(\mathbf{r}, \omega), \tag{1}$$

where D associates with the cosine of the scattering angle g and optical properties, and can be referred to as diffusion equation. $\phi(\mathbf{r}, \omega)$ is radiance at position \mathbf{r} , the light modulation frequency is given by ω , μ_a is the absorption coefficient, c denotes the speed of light in the medium, and the source term is $S_0(\mathbf{r}, \omega)$. D can be expressed as

$$D = \frac{1}{3[\mu_s(1-g) + \mu_a]} = \frac{1}{3(\mu_s' + \mu_a)}, \tag{2}$$

Computationally, the DE may be calculated by the finite element method (FEM) with the absorption and reduce scattering coefficients' exact values along with the light radiance from the NIR laser source $S_0(\mathbf{r}, \omega)$ and the boundary condition. Furthermore, the forward problem equation can be obtained in a complete form using a discrete matrix model with the Galerkin method [43],

$$\begin{bmatrix} A_{ij}^{bb} - \alpha A_{ij}^{bb} & A_{ij}^{bl} \\ A_{ij}^{lb} & A_{ij}^{ll} \end{bmatrix} \begin{Bmatrix} \phi_j^b \\ \phi_j^l \end{Bmatrix} = \begin{Bmatrix} S_j^b \\ S_j^l \end{Bmatrix}, \tag{3}$$

where α refers to the incorporated reflection as a result of the refractive index difference at the boundary, A denotes the optical property matrix, b denotes the boundary node, l is the internal node, and i and j are matrix indexes. Thus, Equation (3) can express the forward model ϕ in the simple matrix form of optical property·boundary light intensity = source radiance.

The reconstructed images can be found by the inverse solution, which minimizes the error in every iteration when the forward problem is completed to be executed. The

distribution $\chi^2 = \|\Delta\phi\|_2^2 = \|\Delta\phi^M - \Delta\phi^C\|_2^2$ can be obtained by minimizing the misfit differences between the photon radiance rate being investigated around the geometry ϕ^M and photon propagation from accomplishing the DE with the initial condition of optical properties ϕ^C . These data–model misfit differences can be minimized by iteratively solving $\mathcal{J}\Delta\chi = \Delta\phi$, where $\mathcal{J} = [\partial\phi^C/\partial\mu_a \ \partial\phi^C/\partial D]$ is the Jacobian matrix and $\Delta\chi$ denotes $[\Delta\mu_a; \Delta D]$, the optical coefficient of the update vector at each iteration. However, solving this inverse problem $\mathcal{J}\Delta\chi = \Delta\phi$ usually involves the difficulty of an ill-posed issue since the model parameters increase. As a consequence, Tikhonov Regularization (TR) was proposed to overcome this problem. Therefore, the DOT inverse problem is expressed as a damped least-squares problem optimization. Hence,

$$\min_{\Delta\chi} \left\{ \|\mathcal{J}\Delta\chi - \Delta\phi\|_2^2 + \lambda^2 \|\Delta\chi\|_2^2 \right\}, \quad (4)$$

is able to be formulated with a regularization parameter λ . When this damped least-squares problem can be minimized iteratively, solving the updated equation can be executed as:

$$\left(\mathcal{J}^T \mathcal{J} + \lambda^2 \mathbf{I} \right) \Delta\chi = \mathcal{J}^T \Delta\phi, \quad (5)$$

where \mathbf{I} refers to an identity matrix [43].

3.2. Near-Infrared Light Source Forms

The reconstructed images of the NIR-DOT measurement are affected by NIR light forms, such as CW, FD, and TD. Three forms of NIR light are shown in Figure 2. The simplest NIR-DOT measure is CW-DOT because it emits a constant light intensity. Generally, to generate a constant light radiance, a direct current (DC) power supply is used to power the NIR after a voltage regulator. The illustration of the CW-DOT measure is depicted in Figure 2a. The light intensity around the tissue boundary can be obtained by the modified Beer–Lambert law (MBLL) [44–46]

$$A = -\log \frac{\phi}{S_0} = \varepsilon CL + S, \quad (6)$$

where A denotes the attenuation corresponding to the optical density, while ε , C , L , and S express molar μ_a , chromophore concentration, mean total pathlength (t-PL), and optical attenuation majorly because of scattering coefficient, respectively. Since CW-DOT simply implements the DC wave to produce a steady intensity, it cannot offer an accurate measurement of the concentration variant. It is reasonable because CW-DOT is unable to penetrate the tissue deeper, and may not accurately evaluate the optical path length resulting in a low resolution of reconstructed images [13,47,48]. Additionally, with the constant input intensity S_0 , the only measured parameter is light radiance around the tissue boundary ϕ . Generally, ϕ has a lower intensity compared to S_0 due to the tissue and defect optical properties. A defect is also known as an inclusion or cancer or tumor in terms of biological tissue.

To overcome the limitation of CW-DOT in measuring the t-PL, FD-DOT and TD-DOT have been implemented, as shown in Figure 2b,c. The meaning of the “frequency-domain” of FD-DOT is derived from the ability to penetrate deeper inside the tissue by producing two outputs, namely light attenuation around the tissue boundary A_O and the phase shift θ_O . Unlike CW-DOT, FD-DOT uses a sinusoidal wave to power the NIR; thus, sinusoidal light is formed. When the input light with an intensity A_I and the phase difference θ_I emit the soft tissue, the light that penetrates gets absorbed, and is scattered toward the tissue. With the difference between the optical properties of the tissue and the defect, one can distinguish the defect location according to the A_O and θ_O . Therefore, the reconstructed images can be defined based on the light intensity and phase shift around the tissue geometry boundary [36,49–51]. An FD-DOT measurement is shown in Figure 2b.

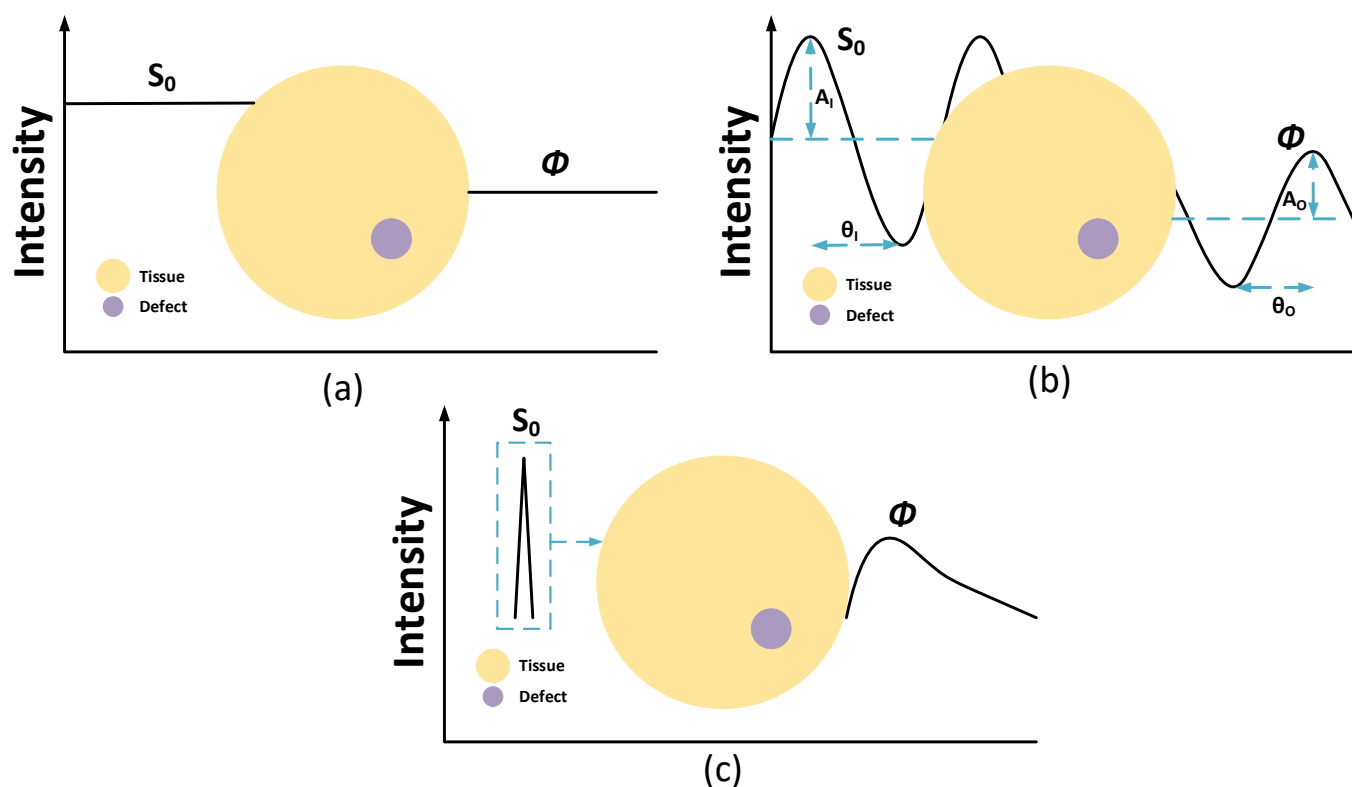


Figure 2. NIR-DOT measurement with (a) CW, (b) FD, and (c) TD. The yellow circle is tissue and the magenta circle is a defect.

The TD-DOT measurement is implied to the ultrashort light radiance of NIR. Normally, this ultrashort time is in a pico-second order. A TD-DOT implements a temporal point spread function (TPSF) to assess the light intensity, as shown in Figure 2c. This method is considered an effective approach to improving DOT spatial resolution because it can verify the mean t-PL by multiplying the mean transit time of the measured photon with the speed of light in the media. Even though TD-DOT may offer better results, its instrumentation and computation are more complicated compared to CW-DOT and FD-DOT [51–53].

4. Near-Infrared Photoimmunotherapy

The three prominent cancer therapies, namely surgery, radiation, and chemotherapy, are to be the mainstays of modern oncology. However, such cancer therapies can trigger undesirable side effects. For instance, cancer surgery may cause bleeding, damage to the surrounding tissue and other organs, uncomfortable pain, infection, slow recovery after the surgery, the risk of metastasis, and residual cancer cells. Meanwhile, cancer radiation treatment has side effects such as fatigue and skin problems at an early stage; during a later term, hair loss, headache, and low blood count may occur. Additionally, chemotherapy's common side effects can be identified as hair loss, sore mouth, anemia, bruising, and bleeding. Thus, to prevent the negative side effects from such common cancer treatments, NIR-PIT emerges to effectively remove cancer [54].

The basic idea of NIR-PIT is to design a special and specific photosensitizer targeting only cancer cells to reduce phototoxicity [23,24]. However, this attempt is not simple, considering past experience with common photodynamic therapies (PDT). The photosensitizer agent often binds with non-targeted areas, such as the skin and other epithelial surfaces, resulting in unnecessary and sometimes unforeseen side effects. Although the specifically designed photosensitizer may spread to the entire body, it is merely acting in the area with the highest light applied. To overcome these common photosensitizer problems, a monoclonal antibodies (mAb)-based photosensitizer is designed and only

activated when there is a bounding with the targeted molecule on the cancer cell membrane and when there is NIR light radiation. These two requirements are essential in the NIR-PIT application [54].

Not only targeting the cancer cell but also the NIR-PIT can initiate a host anticancer immune response; thus, immunosuppressor cells (T-cells) can magnify the targeted cancer cells' immunogenic cell death (ICD), leading to metastatic tumors. Therefore, although cancer cells cannot be eradicated by direct mAb-NIR, NIR-PIT may activate the host anticancer immunity and long-term immune memory without the systemic autoimmune adverse effects. Figure 3 illustrates the NIR-PIT mechanism to activate the host anticancer immunity. The NIR-PIT effect in ICD is to stimulate the immature dendritic cells' maturation in the cancer cells' microenvironment.

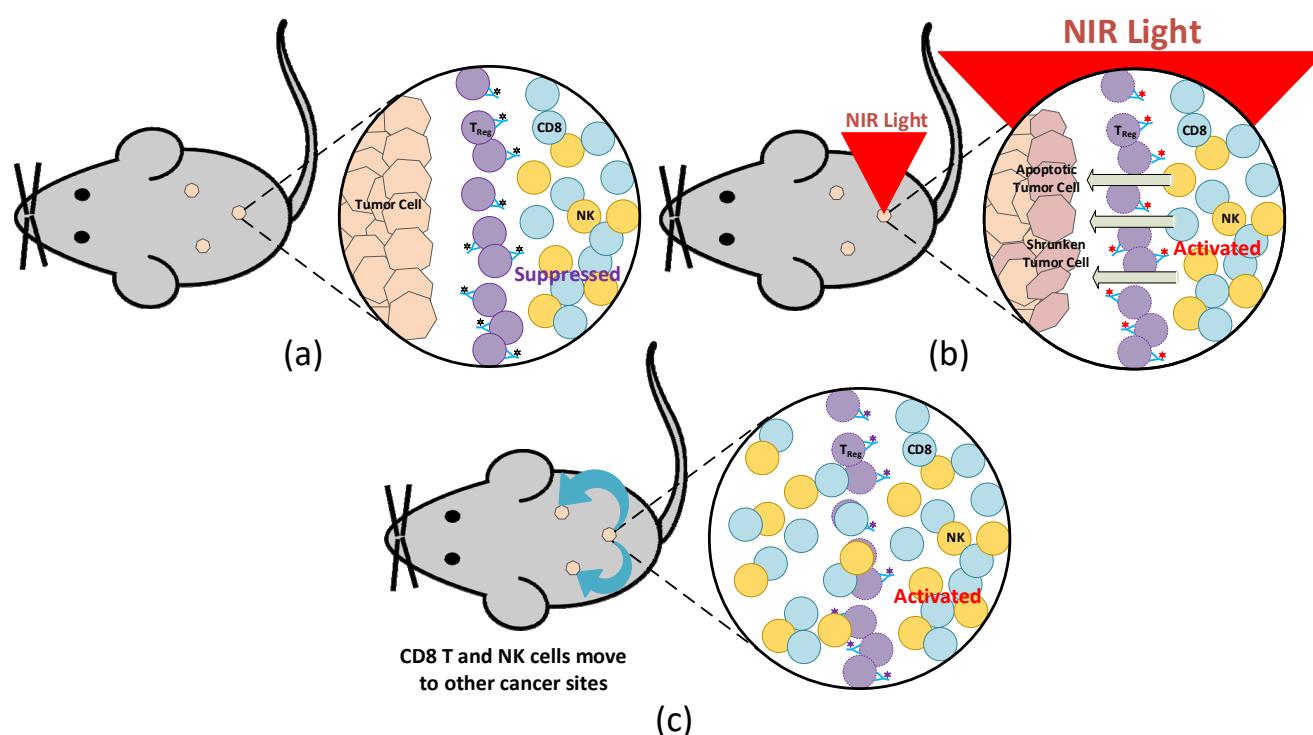


Figure 3. Mice model illustration with NIR-PIT: (a) before and (b) after NIR light irradiation, as well as (c) when CD8⁺ T and NK cells migrate to other cancer sites.

After cancer-cell-targeted NIR-PIT, the primed cluster of differentiation (CD)⁸⁺ T cells respond to a larger repertoire of cancer antigens compared with CD8⁺ T cells prior to NIR-PIT and replicated in treating the tumor. Hence, host anticancer immunity is reinforced once cancer-cell-targeted NIR-PIT, largely due to the reorientation and successive proliferation of CD8⁺ T cells. Even though cancer-targeted NIR-PIT cannot instantly destroy the whole cancer cells in a tumor, the host immune response is available to kill a great proportion of the residual cells, at least in several instances. Consequently, NIR-PIT can have an advantage in completing the suppression of the tumor after one or two therapies. CD8⁺ T and natural killer (NK) cells in treating the tumor are fully initiated within a few hours after the weakening of regulatory T cells (T_{reg}) with NIR-PIT. This T_{reg} -targeted NIR-PIT affects non-treated tumors even though the treatment is addressed at only one targeted lesion. Figure 3a depicts a mice model with embedded tumors when mAb has bounded with T_{reg} , while Figure 3b illustrates the mice model with NIR light irradiation affecting the activation of CD8⁺ T and NK cells to stimulate apoptosis and shrinkage of the cancer cells. Moreover, Figure 3c demonstrates the migration of CD8⁺ T and NK cells to other sites of the tumor to treat non-targeted cancer cells.

The first NIR-PIT system was established in 2011 in the report by Mitsunaga et al. [54]. They used IR700 conjugated with mAbs and pointed to the epidermal growth factor receptors. This in vivo study was conducted by observing the mice model with the implanted tumor. Tumor shrinkage occurred after irradiation with NIR light in target cells. Their results indicate limited success in eradicating a tumor with mAb-IR700 conjugation, but they showed that on one hand, the most effective result is when mAb is bound to the cell membrane and on the other hand, this treatment generated no phototoxicity without bounding. Eight years later, Kobayashi et al. [25] conducted the first human trial using NIR-PIT with cetuximab-IR700 (RM1929) targeting EGFR for surgery incapability in recurrent head and neck cancer patients.

Compared to other traditional photodynamic therapies, which use a special drug, called a photosensitizing agent, in activating the light to kill the cancer cell, NIR-PIT is a targeted phototherapy based on infusing a conjugate of NIR light [55–57]. Thus, NIR-PIT can selectively target the cancer cell by activating the immunogenic cell death of targeted cancer cells. In contrast, non-targeted photosensitizers of common photodynamic therapies are also administrated to the normal tissue and cause various side effects, such as a toxicity effect, even though the light radiation is not harmful.

5. Diffuse Optical Imaging Progress

5.1. Multi-Frequency NIR-DOT

Multi-frequency DOT was first implemented by Intes and Chance in 2005 [58]. They investigated the effect of multi-frequency when the reconstruction algorithm was executed to obtain the distributions of optical properties. In other words, they instantaneously used a set of frequencies in the inverse solution to cast the forward problem. The frequencies they used spanned from 20 MHz to 500 MHz; hence, they had 13 frequency combinations in total. They conducted their experiment by ascending and descending the number of frequencies, for instance, 3, 5, 7, 9, 11, and 13 frequencies or 13, 11, 9, 7, 5, and 3 frequencies. Moreover, the frequency range difference was 40 MHz; thus, for example, in the three-frequency computation, they used 20, 60, and 100 MHz, concurrently. Then, in terms of 13 frequencies, they applied 20–500 MHz. They claimed that a few improvements in reconstructed images can be acquired with more than seven modulation frequencies. Ten years later, in 2015, the second attempt of multi-frequency DOT was performed by Chen et al. [59]. Compared to Intes and Chance's results, Chen et al. confirmed that their method can significantly improve the reconstruction accuracy with only a two-frequency combination, such as 100 + 150 MHz. In their study, they applied three combinations of multi-frequency, namely, 100 + 150 MHz, 100 + 150 + 200 MHz, and 100 + 150 + 200 + 250 MHz and compared them with a single frequency, 100 MHz. In addition, to overcome the TR deficiency, they created a clustered sparsity reconstruction (CSR) algorithm for the inverse problem. They found that only two frequencies are adequate to improve the spatial resolution and with more frequency it is difficult to distinguish the enhancement.

From the abovementioned studies, multi-frequency is one of the schemes that can enhance the resolution and contrast of the reconstructed images. Therefore, they motivated several studies using multi-frequency DOT in improving the reconstructed image quality [60–62]. Evidently, multi-frequency NIR-DOT is associated with the FD-DOT because this measurement relies on the modulation frequency to perform soft tissue imaging. In general, multi-frequency DOT is similar to single-frequency DOT. Nonetheless, the difference between them is that, on the applied frequency, single-frequency DOT is simply using one frequency to modulate the NIR laser light source, such as 100 MHz, as a common modulation frequency, while multi-frequency DOT may implement more than one frequency to modulate the NIR light. These frequencies can be performed individually and the measurement results are combined to obtain the optical distribution when an inverse solution is executed. Moreover, the NIR lasers with various modulation frequencies emit the tissue simultaneously and the measured light is cited to acquire a map distribution of optical properties.

In 2019, Wang et al. investigated a frequency sweep modulation technology to measure the optical parameters inside biological tissue using NIR diffuse photon density waves (DPDW) [63]. They assessed their system performance with an absolute error and correlation coefficient as the evaluation schemes. They verified their DPDW device with an intra-lipid solution and solid phantom to check the accuracy of measured optical properties when compared to true optical parameters. They prepared their phantom study with a geometric size of 200×100 mm, SD distance of 17 mm, $\mu_a = 0.975 \text{ cm}^{-1}$, and $\mu'_s = 5.953 \text{ cm}^{-1}$. Then, they measured the waveform variations of amplitude and phase shift in the range of 300 kHz–1 MHz using an adjustment of frequency step at 7 kHz. Overall, they had 101 frequencies to perform the entire experiment. They speculated that their method with multi-frequency can calculate optical properties faster, more accurately, and simpler than single-frequency methods. Their results showed an absolute error of $\mu_a = 0.019\text{--}0.282 \text{ cm}^{-1}$ and $\mu'_s = 0.002\text{--}0.003 \text{ cm}^{-1}$. These results indicated that multi-frequency can amplify the deeper penetration of the light to yield more information regarding optical parameters, implying better-reconstructed images.

5.2. NIR-DOT Incorporating Other Modalities

DOT based on NIR has several shortcomings when inspecting biological tissue. Whether it is with NIR-I or NIR-II, DOT is still considered challenging to precisely detect the presence and location of inclusion because it can only penetrate several centimeters into the tissue. The light intensity is diminished following the deeper light propagation into the tissue and soon the light attenuation is below the detection margin.

Combination with other imaging modalities to improve the DOT performance may provide a better result. With the emergence of non-invasive imaging modalities, patients can avoid unnecessary medical treatment, such as biopsy [64]. Indeed, NIR-DOT can be combined with X-ray, MRI, ultrasound (US), and computed tomography (CT) scan [11,65,66]. Two well-known combinations of DOT with other imaging modalities are MRI-guided DOT and US-guided DOT [65,67]. With the assistance of an MRI and US, NIR-DOT may enhance the spatial resolution because it can receive prior information related to the functional or structural information of the biological tissue. For instance, the concentration and saturation of hemoglobin can be acquired and high-resolution structural imaging and improved gadolinium contrast (Gd-contrast) can be validated by MRI. Additionally, NIR-DOT may be used as an additional method to investigate the functional condition. Certainly, in the case of MRI and DOT combinations, MRI can act as a method to measure indirect and low sensitivity of the deoxy-hemoglobin, whereas DOT can directly evaluate oxy- and deoxy-hemoglobin with higher sensitivity. In this term, DOT offers validation and augmentation of hemodynamics measures [65].

Furthermore, MRI-DOT can be further developed toward MRI-CW-DOT and MRI-TD-DOT, as introduced by Cochran et al. [42] in 2019. Their method was developed to improve the functional optical properties' quantification and lesion localization in the diagnosis and prognosis of breast cancer. To achieve their goal, they required CW and TD techniques to provide three-dimensional (3D) tomography incorporating spectroscopic measurement of blood flow. They had six pulsed NIR lasers (< 70 ps) for TD measurement with 690, 750, 780, 798, 838, and 905 nm and five continuous NIR lasers for CW measurement with 670, 785, 808, 850, and 915 nm. To implement the laser diode, they placed a 12×1 wavelength switch preceding the light sources. They used two detectors to cite the light intensity, namely CCD cameras with fibers at the 108-degree position for CW and PMT located at the 8-degree position for TD measurement. They performed the MRI and DOT simultaneously because DOT does not affect the magnetic field; however, they performed CW and TD separately. In general, two tissue structure images were created before Gd-contrast agent injection to acquire another new set of MR images. Furthermore, the TD-DOT was accomplished first to ascertain the absolute bulk of μ_a and μ_s . Then, to obtain a full 3D reconstruction, CW-DOT was executed for completing the experiment.

5.3. Deep-Learning-Based DOT Image Reconstruction

A traditional inverse solution with TR to predict optical properties' distribution inside the tissue may lead to overestimation and over-smoothing of the area of the region of interest (ROI). This often offers imprecision in the predicted contrast in the reconstructed images. To overwhelm this disadvantage of NIR-DOT, the discriminative model of artificial neural network (ANN), such as convolutional neural network (CNN), were sought to provide a solution to quantify more precisely the reconstructed optical parameters [68,69]. Two general approaches that were developed for NIR-DOT image reconstruction are the CNN-based inverse model to accurately reconstruct the optical properties and the autoencoder model to minimize the noise from reconstructed images [70–72]. Additionally, as for tumors, CNN can also be used to classify the DOT-reconstructed images into non-cancerous and cancerous [73–75].

To categorize breast cancer into benign and malignant groups using the DOT imaging system, in 2019, Xu et al. [76] developed a system as a computer-based observer based on CNN for automatically classifying breast mass lesions. To collect the dataset, they imaged 63 breast cancer patients with NIR-DOT; thus, they compiled a database of 1260 two-dimension (2D) grayscale images in total. They prepared their CNN model with two convolutional layers, two batch normalization layers, and one fully connected layer by assigning a sigmoid activation function to predict the cancer malignancy status. The original dataset had 860 benign images and 400 malignant images. First, they classified the images without data augmentations using 645 benign training images and 300 malignant training images. The model was tested after training utilizing 215 benign images and 100 malignant images. Ultimately, they obtained an accuracy of 90.2%, specificity of 0.80, sensitivity of 0.95, and area under the receiver operating characteristic (ROC) curve (AUC) of 0.94. Additionally, to improve their CNN model operation, they augmented the original dataset; hence, they had 860 benign images and 700 malignant images. They split this dataset into 645 benign training images, 600 malignant training images, 215 benign test images, and 100 malignant test images. With the data augmentations, they were able to improve their results to an accuracy of 93.3%, specificity of 0.88, sensitivity of 0.99, and AUC of 0.95.

An implementation of deep learning for NIR-DOT-reconstructed images has been accomplished by Balasubramaniam et al. [71]. An anomaly can be recognized by an autoencoder model because, in principle, it contains encoder and decoder networks to reduce the noise in the reconstructed images. An autoencoder is developed for minimizing the image pixel by maintaining its quality. In advance, an autoencoder may provide noise reduction to obtain adequate image quality. Further, a U-Net model inspired by the autoencoder concept has been developed for anomaly detection [77]. Thus, deep learning may provide superior image reconstruction results compared to a traditional method.

6. Near-Infrared Photoimmunotherapy Progress

6.1. NIR-PIT Principle and Instrumentation Progress

A recently created cancer treatment called NIR-PIT uses an antibody coupled to the silicon phthalocyanine dye IRDye700DX, which absorbs NIR light (IR700) [23]. After being injected intravenously, this antibody–photo-absorber conjugate (APC) attaches to particular cancer cells that express the correct antigen on their cell membrane [78]. Then, NIR light is focused on the tumor to activate the APC and cause cell death. The axial ligands of the IR700 molecule, which are in charge of the molecule's hydrophilicity, disassociate from the main molecule as soon as it is exposed to NIR light, which causes the APC to transform from a highly hydrophilic compound to a highly hydrophobic compound [79]. This alteration in the APC's chemical composition encourages aggregation, which weakens and ruptures the cellular membrane [80]. The cell membrane gradually becomes more permeable, microperforations develop, and eventually blebbing and bursting take place, leading to necrotic cell death. This method of cell death clearly sets NIR-PIT apart from traditional photodynamic treatment (PDT), which depends on the generation of reactive

oxygen species to harm nearby normal tissue non-selectively [81]. In theory, because NIR light can only penetrate as far as 2 cm below the tissue surface, NIR-PIT is best suited for treating superficial cancers [82]. NIR light can go significantly further through the air in the lungs under specific conditions, such as when treating cancers in the lung and pleural cavity [81]. The light source must be positioned inside or close to tumors because NIR light is rapidly attenuated in more solid tissues. Flexible, cylindrical, fiber optic, interstitial light diffusers that are placed into the treatment site can be used to achieve this [23]. Practically any tumor site is susceptible to NIR-PIT when implanted via needle, catheter, or endoscope using interstitial light diffusers [83]. Furthermore, it is possible to continuously produce light in a distant tumor site using implanted wireless NIR-light-emitting diode (LED) sources [7]. Fluorescence imaging can be utilized to identify tumor areas to which the APC is bound and to deliver therapeutic doses of light to those fluorescing regions because the IR700 is both a therapeutic and a diagnostic device [84]. After the dye has been totally photobleached, there is a minimum plateau in fluorescence, which decreases as the light photobleaches the IR700. According to reports, the degree of photobleaching correlates with the therapeutic impact [24]. Due to the high intensity of the excitation light and the extended emission spectrum of IR700 during NIR-PIT, a commercially available camera that was initially intended to image indocyanine green, which typically operates at wavelengths of 830 nm, can now be used to detect the low-level fluorescence resulting from IR700 [23]. This makes it possible to continuously monitor NIR-PIT at wavelengths different from the powerful laser excitation light at 690 nm. NIR-PIT is unusual in that it causes immunogenic cell death, in contrast to the majority of cancer therapies that result in apoptotic cell death (ICD). ICD is a form of cell death where the immune system's adaptive response is triggered by a flood of cell-associated antigens released by cancer cells that have been injured [23]. The adaptive immune system is not activated by apoptotic cell death. Danger signals such as calreticulin (CRT), adenosine triphosphate (ATP), high-mobility group box 1 (HMGB1), heat shock protein (Hsp) 70, and Hsp 90 are released, which triggers the ICD [85]. These danger signals increase the presentation of tumor antigens to T cells and activate immature dendritic cells (DCs). Cancer cells treated with NIR-PIT emit HMGB1, ATP, and CRT as death signals. In addition, the activated DCs absorb cancer-specific antigens released from the burst tumor cells, maturing into DCs that can prime and instruct naive T cells to become CD8⁺ T effector cells that specifically target cancer [80]. Some non- or low-immunogenic cancers have been proven to become immunogenic tumors when treated with NIR-PIT, which works by using innate immunity to detect recently produced cancer-specific antigens. Patients with recurrent head and neck malignancies are currently being investigated in a global Phase 3 clinical trial employing an anti-epidermal growth factor receptor (EGFR) antibody conjugated to the IR700 molecule (Cetuximab-IR700). Fast-track recognition for NIR-PIT has been granted by the US Food and Drug Administration (FDA) [25]. Additionally, the Pharmaceuticals and Medical Devices Agency in Japan granted provisional approval and registered for clinical use the first EGFR-targeted NIR-PIT medication (ASP-1929; AkaluxTM, Rakten Medical Inc., Tokyo, Japan) and a diode laser system (BioBladeTM, Rakten Medical Inc., Tokyo, Japan) in September 2020 [23]. Studies involving NIR_PIT for cancer treatment since 2014 are given in Table 1.

Table 1. NIR-PIT cancer therapy works.

Paper	Year	Application	Setup
Shirasu et al. [86]	2014	Carcinoembryonic antigen-expressing tumor	IRDye700DX
Sano et al. [87]	2014	Epidermal growth factor receptor (EGFR)-positive A431 cells	Monoclonal antibody (mAb)-photosensitizer (IR700 fluorescence dye)
Kazuhide et al. [88]	2014	HER2-expressing, GFP-expressing, gastric cancer cell line (N87-GFP)	Photosensitizer, IR-700, conjugated to trastuzumab (tra-IR700)

Table 1. Cont.

Paper	Year	Application	Setup
Nagaya et al. [82]	2015	Breast cancer	Cetuximab (cet)-IR700
Hanaoka et al. [89]	2015	Hepatocellular carcinoma	IR700-conjugated antibodies
Sato et al. [90]	2015	Ovarian cancer	IRDye-700DX
Sato et al. [81]	2015	Lung carcinoma	IRDye-700DX
Jing et al. [91]	2016	Brain tumors	Monoclonal antibody (mAb)-phototoxic phthalocyanine dye IR700 conjugates
Nagaya et al. [78]	2016	Mesothelin-expressing tumors	hYP218-IR700
Nagaya et al. [92]	2016	B-cell lymphoma	Monoclonal antibody (mAb), rituximab-IR700
Railkar et al. [93]	2017	Bladder cancer	IRDye 700Dx (IR700)
Nagaya et al. [84]	2017	Prostate cancer	Monoclonal antibody (mAb), conjugated to the photo-absorber, IR700DX
Nagaya et al. [94]	2017	Lung adenocarcinoma	Monoclonal antibody (mAb), avelumab, conjugated to the photo-absorber, IR700DX
Nagaya et al. [95]	2017	Oral cancer	Monoclonal antibody (mAb), avelumab, conjugated to the photo-absorber, IR700DX
Ogawa et al. [85]	2017	HER2 expression	Tra-IR700 or Cet- IR700
Burley et al. [37]	2018	Glioblastoma treatment EGFR	IR700DX
Siddiqui et al. [96]	2019	Bladder cancer	Monoclonal antibodies (MAbs) conjugated to a photoabsorber (PA), IR Dye 700Dx
Kiss et al. [97]	2019	Bladder cancer	anti-CD47-IR700
Lutje et al. [98]	2019	Prostate cancer	Anti-PSMA monoclonal antibody D2B was conjugated with IRDye700DX and DTPA
Watanabe et al. [99]	2019	Human esophageal squamous carcinoma	Fibroblast activation protein (FAP)-IR700
Wei et al. [100]	2019	Melanoma	IR700-YY146
Nagaya et al. [101]	2019	Gastric cancer	Trastuzumab (tra)-IR700DX
Nakamura et al. [102]	2019	Bone cancer	IRdye 700DX
Nagaya et al. [80]	2019	Colon cancer	IR700-conjugated anti-CD44 anti-CD44
Isobe et al. [83]	2020	Lung cancer	Rova-IR700
Maruoka et al. [103]	2020	Colon cancer	Anti-CD44-IR700
Katsube et al. [104]	2021	Esophageal cancer	Fibroblast activation protein (FAP)-IR700
Okada et al. [105]	2021	Colon cancer	IR700 conjugated with anti-CTLA4

6.2. NIR-PIT Enhances Anticancer Host Immunity

The main benefits of NIR-PIT are killing tumors without destroying the surrounding normal cells and enhancing the host immune system to continue removing the cancer cells after NIR light radiates the ICD that initiates against the targeted cancer cells. NIR-PIT-treated cancer cells distribute death signals containing adenosine-triphosphate (ATP), calreticulin, and high-mobility group box 1 (HMGB1) regulator [24,106]. These signals activate the maturation of immature dendritic cells (DCs) that consume cancer-specific antigens, which are distributed from the cracked tumor cell. Then, these mature DCs set up and instruct naive T cells to develop into cancer-specific CD8⁺ T cells. These prepared cancer-specific CD8⁺ T cells reproduce and strike other cancer cells, causing an expanded host antitumor immune response. These subsequent activities could transform several non-immunogenic tumors into immunogenic tumors by identifying enormously released neo-antigens. Following the CD8⁺ T and NK cells fight, the cancer cells migrate to other cancer sites, even though the other cancer sites are not injected by mAb. This antitumor immune activation appears initially in the treated tumor site, but ultimately continues to other cancer spots since immune cells drift all through the body, developing a systemic

immune response. Hence, although NIR-PIT is a local therapy, the impact of NIR-PIT can be systemic and could influence remote metastatic sites.

6.3. CD29-Targeted NIR-PIT

NIR-PIT is perfect for surface skin cancers, for instance, melanomas. Recently, Furusawa et al. [22] examined the efficiency of CD29-PIT and CD44-PIT in the B16-F10 melanoma model, which is highly pigmented. They started their experiment by preparing the AbPC. They synthesized the AbPC with 6.7 nmol of anti-CD29 and anti-CD44 antibodies, which were incubated with 34.2 nmol of IR700 NHS ester (Li-Cor) in 0.1 M Na_2HPO_4 solution with a pH of 8.5 for 1 h at room temperature. The mixture was sterilized using a PD-10 Desalting Column with Sephadex G-25 resin (Cytiva) and eluted with PBS. The resulting AbPC solution was diluted to make 1.675 nmol/mL. The same quantity of unconjugated antibodies was inserted beside the AbPCs as control. They performed their experiment in vitro and in vivo. In an in vitro environment, they seeded B16-F10 (B-16) cells in a 24-well plate at 0.1×10^6 cells/well a day before the experiment. The in vitro results demonstrated that CD29 expression was negatively associated with cell density, whereas CD44 expression was positively correlated to cell density. This expression form implied that CD29 expression was greater in the more proliferative subset of B16 cells, whereas CD44 expression was elevated in the fewer proliferative subset of B16 cells. Additionally, for the in vivo experiment, they found that CD29 expression was naturally consistent throughout the tumor, including the edge; meanwhile, CD44 was normally stated in a gradient that lessened toward the tumor edge. CD29 expression was noticed mutually in the cytoplasm and on the cell membrane, while CD44 expression was found only on the cell membrane. Moreover, they checked the effects of CD29-PIT and CD44-PIT on the surrounding normal skin. The results indicated that they are safe for normal skin cells. To complete their experiment, they investigated the condition of the remaining cancer cells. They combined CD29 + CD44-PIT to obtain better results when fighting against the cancer cells. However, the survivor cancer could not be destroyed by these two targets. Furthermore, the cancer survivor cells finally grew back, although CD29-PIT-treated tumors grow back slower. CD29-PIT was more competent compared to CD44-PIT because the survivor cells of CD29-PIT were less proliferative compared to CD44-PIT. Additionally, they investigated the effects of CD29-PIT and CD44-PIT on the immune cells. CD29-PIT did not damage the immune cells during treatment, while CD44-PIT kills NK and DCs.

6.4. Combined Photothermal-Immunotherapy

NIR-PIT cancer treatment may not remove the entire set of cancer cells from the patient's body. Thus, the modality combination of the cancer treatment is vital to improving cancer cell death. A novel combination of photothermal and photoimmunotherapy was established by Lv et al. [77] in 2021. They developed an anticancer platelet-based biomimetic formulation (N+R@PLTs) that integrates photothermal nanoparticles (N) and immunostimulator (R) into thrombocytes. They synthesized photothermal polymer nanoparticles by incorporating thiophene and naphthalene diimide moieties into the polymer skeleton. Their designed photothermal polymer exhibited slight cytotoxicity to healthy cells, which did not guarantee safety when governing them in vivo. To utilize the photothermal nanoparticles with supplementary proplatelet (PLT) sensitivity and immunogenicity, the nanoparticles were later embellished with biotin, whereas CD42a on the PLT membrane was pre-treated with avidin-labeled anti-CD42a antibody. The experiment showed that a few N+R@PLTs spread to the tumor sites within 1 h and gradually increased until 8 h of observation. With this examination, they claimed that there is colocalization of N and R signals in immunohistochemical (IHC) tumor segments. Moreover, the temperature quickly increased to 56°C in the N+R@PLT group causing the highest expression of heat shock protein (HSP) in tumor tissue. With their formulation, they could create more tumor antigen (TA) signals in DCs. Consequently, more CD8^+ T cells from the immunostimulatory tumor-draining lymph node (TLN) penetrated the cancer cells producing apoptotic cancer. In general, their results

implied an exceptional immunotherapeutic outcome that complemented the photothermal therapy operation.

7. NIR Challenges

The appropriate spatial resolution needed for the real-time monitoring of immunological components is provided by NIR imaging [18]. The performance of labeling agents, however, heavily depends on the fluorophores used because of their optical and physicochemical properties, such as hydrodynamic diameter, molecular weight, absorption/emission wavelengths, surface charges, hydrophobicity, plasma protein binding, and photostability [63]. Important characteristics include high imaging specificity for tracking the targeted immune components, high imaging sensitivity for detection (reduced non-specific uptake), non-immunogenicity, and low toxicity, which should be present in the optimal imaging probe for labeling the immune components of interest [107]. Longitudinal monitoring of *in vivo* cell proliferation is possible through the transfection of cells with fluorescent proteins, such as biological green fluorescent protein [85]. However, it can be challenging to get sufficient fluorescence density quickly enough after injection, and the use of virus infection restricts their ability to be used in clinics. Hence, small molecule fluorophores and fluorescent nanoparticles are sought [83]. Cellular mobility and immunogenicity may be hampered by the inclusion of cell tracking dyes (small molecule fluorophores) because of changes in cellular mechanical properties including stiffness and adhesion brought on by an increase in the lateral contact between phospholipid chains and amphiphilic dye molecules [83]. Nanoparticles show considerable promise to overcome the limited sensitivity, chemical degradation, and photobleaching of organic fluorophores in cell labeling, in contrast to small-molecule fluorophores [7]. Nanoparticles can carry significant payloads in addition to contrast agents and can be further modified in terms of their optical, electrical, magnetic, and biological properties. Nanoparticles are typically more amenable to broader approaches for bioimaging and tissue targetability than small molecules, despite the fact that this method has a number of significant drawbacks, including the complexity of their design, high cost, difficulty in large-scale production, and, most importantly, the unknown long-term toxicity to biological systems [2,108]. The majority of *ex vivo* labeling with nanoparticles depends on cells' inherently strong endocytosis activity, particularly that of macrophages [7]. In addition to endocytosis, other methods such as transfection, microinjection, and electroporation have also been developed. However, this comes at the expense of high cost and sophisticated technology [109].

The other important challenge in NIR application is miniaturization [6]. In the NIR applications to cancer investigations, fiberoptic probes are crucial. The optical characteristics of the tissue and the source-detector spacing determine the greatest depth of photon penetration in the tissue (by a larger separation an enhanced tissue depth is probed). The probe design is crucial in acquiring tissue information since the source-detector geometry greatly influences the depth and volume of the tissue that is being probed, particularly in depth-resolved research [110]. Spectral information, specific to each layer in the tissue, can disclose information on disease development if distinct layers in the tissue are targeted selectively by an optimized source-detector geometry. Different organizations have utilized a wide variety of source-detector geometries for NIR studies of cancer. Large source-detector separations and somewhat lengthy route lengths have been used in many of these experiments. As a result, the retrieved optical properties represent average values over a sizable tissue volume, and the detected photons have traveled a considerable distance through the tissue. As a result, the optical approaches are less sensitive to modifications in the epithelial tissue layer. In order to compensate for this, studies focusing on tissue microenvironment are ongoing. This challenge should be addressed as it is crucial to understanding tissue microenvironment changes.

The extremely selective necrotic/immunogenic cell death that NIR-PIT causes in the targeted tumor cells encourages dendritic cells' maturation and sets up cytotoxic T cells to respond to cancer-related antigens released from dead cancer cells [80]. Due to the heightened host tumor immunity brought on by the initial antitumor NIR-PIT, when NIR-

PIT is paired with an immuno-checkpoint inhibitor or NIR-PIT targeting Treg, NIR light not only exposes local cancers but also distant metastatic tumors [23,25,80]. In human studies, this “vaccine-like” quality of NIR-PIT needs to be investigated.

Another concern is that research is now being conducted to determine the best NIR-PIT treatment plan for various tumor types [99]. The distribution of immune cells with antitumorigenic effects and other tumor-infiltrating lymphocytes with pro-tumorigenic effects in the tumor microenvironment may play a significant role in the selection of optimum patients and ideal NIR-PIT combos. To find the best NIR-PIT combo technique for each type of tumor, more research is required.

8. NIR Research Future Directions

8.1. Improved NIR_DOT

The three schemes that may amplify the performance of NIR-DOT are multi-frequency DOT, the combinations of DOT with other imaging modalities, and deep-learning implementation. However, numerous techniques may emerge to validate DOT’s capability and effectiveness. A simple approach to improve DOT is to change the number of SD pairs. With the variation of SD, the light excited can increase in amount; thus, the measured light around the tissue boundary can have various accuracies. Additionally, NIR-II implementation for DOT is rare; hence, a wide window of opportunity is laid out for researchers. Multi-wavelength is also interesting to undergo since it extends the DOT measurement from only inclusion detection to oxy-, deoxy-hemoglobin, and lipid concentrations prediction.

Another attractive area is to find a novel method to overcome the limitation of inverse solution in terms of regularization. Naturally, the reconstruction algorithm is ill-posed; thus, an improvement can be achieved if an appropriate regularization is employed. Moreover, in the simulation field, the mesh generation algorithm is essential because it accurately computes the photon migration model in the forward problem and precisely predicts the optical properties distribution. With a well-structured mesh, the position of SD can be managed well and applied in the clinical environment. Additionally, to avoid the inverse problem, the number of voxels, nodes, and elements should be different between forward and inverse solutions. Therefore, mesh generation is to be the main step to developing accurate NRI based imaging. Due to the complexity of the full 3D computation of DOT, a proper mesh arrangement leads to an effective computational cost. The higher number of voxels, nodes, and elements, the longer the computational time.

8.2. NIR-Based Cancer Suppression Instrumentations

This section describes the prospective instrumentations for cancer suppression using NIR. We first discuss the probability of establishing instrumentations in an in vitro environment. We show our speculation of these prospective instrumentations based on the published articles that use visible light, ultrasound, or their combination to control cancer group growth [111–115]. Unlike their implementation using visible, ultrasound, or their combination, here, we attempted to discuss future approach to construct an NIR system for suppressing cancer reasonably with combined NIR-I and NIR-II, NIR and visible light, NIR along with ultrasound, and various wavelengths and frequencies, as well as CW, FD, and TD implementations.

The first possibility to generate NIR cancer suppression-based instrumentation uses single-wavelength NIR with adjustable power sources and waveforms. Figure 4 depicts the mechanism of single-wavelength NIR with four different waveforms. The power supply provides the voltage to activate the waveform generator. In the waveform generator component, one can select the preferred waveform, such as sinusoidal, rectangle, triangle, and pure DC voltage to power the NIR laser/light-emitting diode (LED) in terms of single wavelength. Indeed, we can generate the waveform ratio with a pulse width modulation (PWM); thus, an adjustable waveform may be produced in the range of 0–100%. A single and integrated waveform, then, illuminates the cancer cell line to control the cancer growth. The system in Figure 4 may be improved by applying multi-wavelength for the NIR measurement.

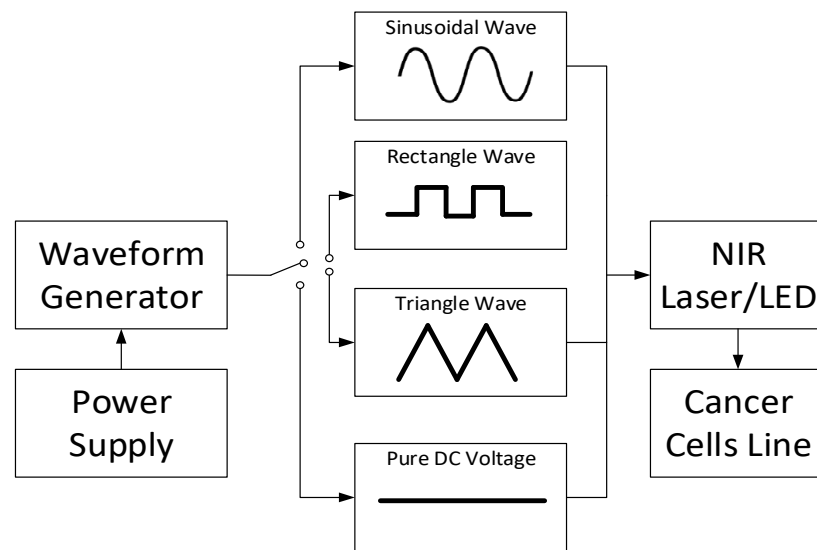


Figure 4. Single-wavelength NIR with four different waveforms instrumentation.

Another instrument may be established using the combination of NIR-I, NIR-II, and visible light, as shown in Figure 5. To provide appropriate voltage to power the NIR-I, NIR-II, and visible light, a power regulator is utilized to arrange the power distribution for each light source. To minimize the power of light intensity and to focus the light radiation, a filter lens for every light source is directed to the light before illuminating the cancer cell line. Subsequently, their combinations may be integrated to enhance the cancer growth control system ability. Moreover, it is possible to assign any visible light to a specific wavelength; then, various NIR-I and NIR-II spectral windows can be implemented to obtain a comprehensive report corresponding to their incorporation.

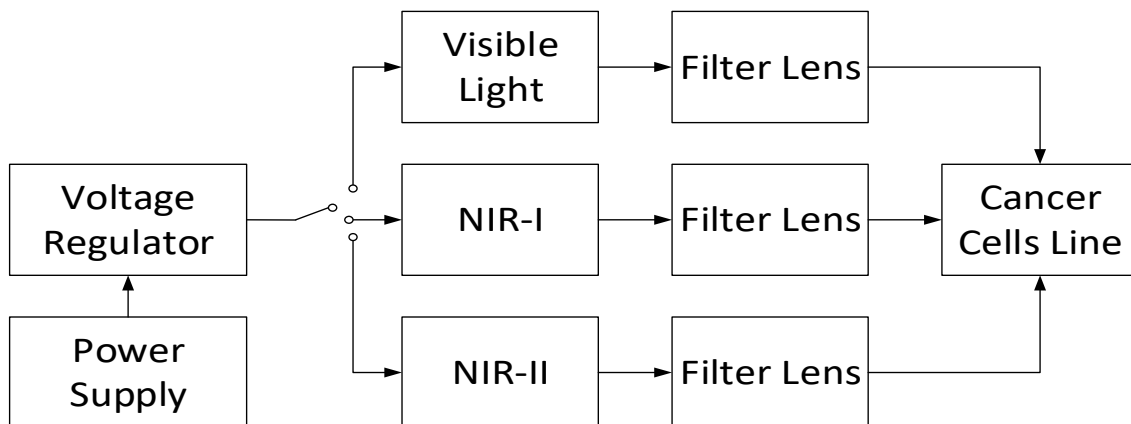


Figure 5. Combined NIR-I and NIR-II with visible light instrumentation.

Moreover, an *in vitro* system can be developed by applying the combinations of NIR-I, NIR-II, and other cancer-suppressor modalities, such as ultrasound, as shown in Figure 6. When other modalities are implemented, a signal conditioner circuit (SCC) is required to generate the ideal signal for such modalities. This SCC can be a function generator, power amplifier, clipper-clamper circuit, ripple reduction circuit, and others. With these combinations, the cancer cells may be eradicated successfully compared to the control group.

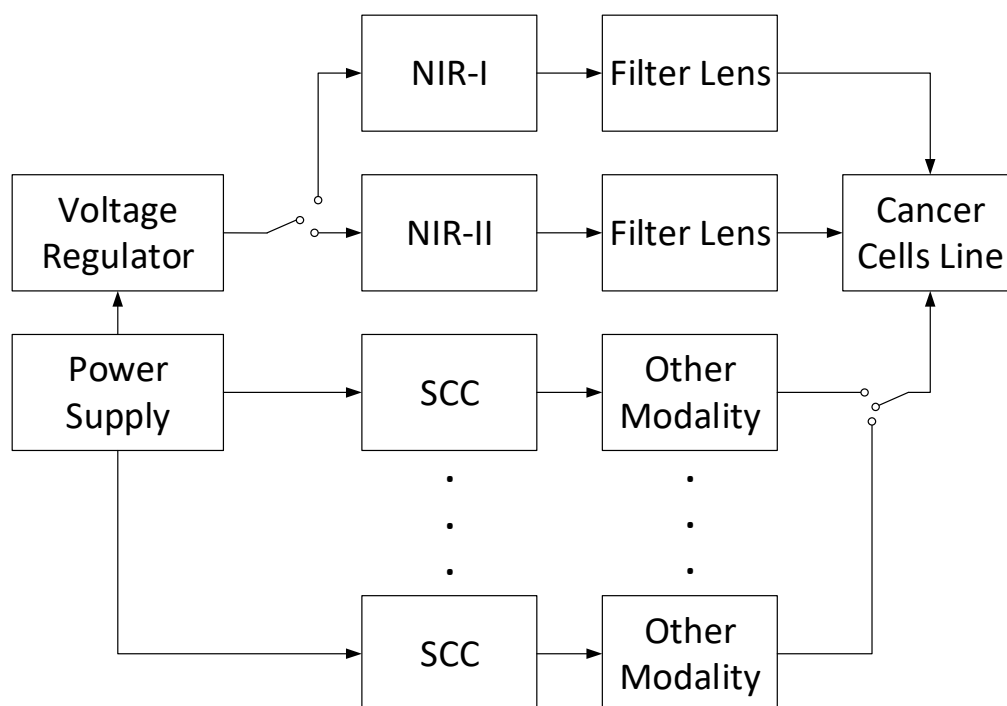


Figure 6. Instrumentation of combined NIR-I and NIR-II along other modalities.

Finally, a novel cancer cell suppressor with the combination of CW, FD, and TD can be designed, as shown in Figure 7. As DOT has demonstrated a promising ability to image the soft tissue with the NIR light penetration, three NIR light types may be applied to establish the cancer cell growth control apparatus. A voltage generator can be implemented to supply appropriate power for each NIR light type. To focus and filter the NIR light for only targeted cancer cells, one can place the filter lens in front of each NIR light source type. The measurement is completed when the comparisons among individual light sources emitting the cancer cell and their combinations are obtained.

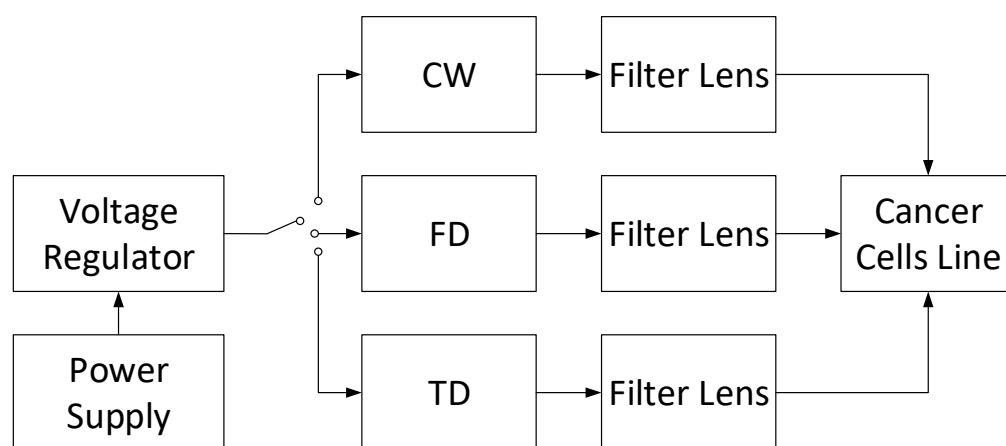


Figure 7. Combined CW, FD, and TD light sources instrumentation.

9. Conclusions

In this review, an overview of near-infrared application in cancer cell imaging and therapy has been discussed. The discussion in this paper focused on instrumentation for imaging and therapy based on NIR. The state-of-the-art research for NIR-based cancer imaging and therapy has been thoroughly reviewed. The challenges that researchers face

in the area of NIR for cancer imaging and therapy have been described. Furthermore, prospective instrumentation to establish cancer therapeutics apparatuses based on near-infrared technology have been presented. In summary, we have observed that most of the studies in the area of NIR's application for cancer imaging and therapy are still in the pre-clinical stages and, given the superiority of the approaches involving NIR, clinical translation should be the focus area of researchers. Moreover, the systemic effect of NIR-PIT should be carefully studied. Additionally, the application of the nanoparticle has brought about improvement in NIR-based studies, but the cost-benefit and toxicity remain a challenge. Finally, the use of artificial intelligence may be leveraged in imaging cancer and support NIR-PIT based treatment.

Author Contributions: Conceptualization, V.M., S.-U.Z. and S.-w.C.; Writing—original draft preparation, V.M. and S.-w.C.; Writing—review and editing, V.M., G.A. and S.-w.C.; Supervision, S.-w.C.; Funding acquisition, S.-U.Z. and S.-w.C. All authors have read and agreed to the published version of the manuscript.

Funding: This work was supported in part by the National Research Foundation of Korea (NRF) Grant funded by the Korean Government (MSIT) [NRF-2019R1F1A1062397], Dong-Eui University Foundation Grant (2022), and project for Industry-University-Research Institute platform cooperation R&D funded by Korea Ministry of SMEs and Startups in 2022 (S3310765).

Institutional Review Board Statement: Not applicable.

Informed Consent Statement: Not applicable.

Data Availability Statement: Not applicable.

Conflicts of Interest: The authors declare no conflict of interest.

References

1. Amineh, R.K. Applications of Electromagnetic Waves: Present and Future. *Electronics* **2020**, *9*, 808. [[CrossRef](#)]
2. Centeno, A.; Aid, S.R.; Xie, F. Infra-Red Plasmonic Sensors. *Chemosensors* **2018**, *6*, 4. [[CrossRef](#)]
3. Erdoes, G.; Rummel, C.; Basciani, R.M.; Verma, R.; Carrel, T.; Banz, Y.; Eberle, B.; Schroth, G. Limitations of Current Near-Infrared Spectroscopy Configuration in Detecting Focal Cerebral Ischemia During Cardiac Surgery: An Observational Case-Series Study. *Artif. Organs* **2018**, *42*, 1001–1009. [[CrossRef](#)] [[PubMed](#)]
4. Karim, A.; Andersson, J.Y. Infrared Detectors: Advances, Challenges and New Technologies. *IOP Conf. Ser. Mater. Sci. Eng.* **2013**, *51*, 012001. [[CrossRef](#)]
5. Zahir, S.A.D.M.; Omar, A.F.; Jamlos, M.F.; Azmi, M.A.M.; Muncan, J. A Review of Visible and Near-Infrared (Vis-NIR) Spectroscopy Application in Plant Stress Detection. *Sens. Actuators A Phys.* **2022**, *338*, 113468. [[CrossRef](#)]
6. Kenry; Duan, Y.; Liu, B. Recent Advances of Optical Imaging in the Second Near-Infrared Window. *Adv. Mater.* **2018**, *30*, 1802394. [[CrossRef](#)] [[PubMed](#)]
7. Li, J.; Duan, H.; Pu, K. Nanotransducers for Near-Infrared Photoregulation in Biomedicine. *Adv. Mater.* **2019**, *31*, 1901607. [[CrossRef](#)]
8. He, J.; Li, C.L.; Wilson, B.C.; Fisher, C.J.; Ghai, S.; Weersink, R.A. A Clinical Prototype Transrectal Diffuse Optical Tomography (TRDOT) System for in Vivo Monitoring of Photothermal Therapy (PTT) of Focal Prostate Cancer. *IEEE Trans. Biomed. Eng.* **2020**, *67*, 2119–2129. [[CrossRef](#)]
9. Hayashi, R.; Yamashita, O.; Yamada, T.; Kawaguchi, H.; Higo, N. Diffuse Optical Tomography Using FNIRS Signals Measured from the Skull Surface of the Macaque Monkey. *Cereb. Cortex Commun.* **2022**, *3*, tgab064. [[CrossRef](#)]
10. Mimura, T.; Okawa, S.; Kawaguchi, H.; Tanikawa, Y.; Hoshi, Y. Imaging the Human Thyroid Using Three-Dimensional Diffuse Optical Tomography: A Preliminary Study. *Appl. Sci.* **2021**, *11*, 1670. [[CrossRef](#)]
11. Hoshi, Y.; Yamada, Y. Overview of Diffuse Optical Tomography and Its Clinical Applications. *J. Biomed. Opt.* **2016**, *21*, 091312. [[CrossRef](#)] [[PubMed](#)]
12. Hernandez-Martin, E.; Gonzalez-Mora, J.L. Diffuse Optical Tomography in the Human Brain: A Briefly Review from the Neurophysiology to Its Applications. *Brain Sci. Adv.* **2020**, *6*, 289–305. [[CrossRef](#)]
13. Doulgerakis, M.; Eggebrecht, A.T.; Dehghani, H. High-Density Functional Diffuse Optical Tomography Based on Frequency-Domain Measurements Improves Image Quality and Spatial Resolution. *Neurophotonics* **2019**, *6*, 035007. [[CrossRef](#)] [[PubMed](#)]
14. Dai, X.; Zhang, T.; Yang, H.; Tang, J.; Carney, P.R.; Jiang, H. Fast Noninvasive Functional Diffuse Optical Tomography for Brain Imaging. *J. Biophotonics* **2018**, *11*, e201600267. [[CrossRef](#)] [[PubMed](#)]
15. Wheelock, M.D.; Culver, J.P.; Eggebrecht, A.T. High-Density Diffuse Optical Tomography for Imaging Human Brain Function. *Rev. Sci. Instrum.* **2019**, *90*, 051101. [[CrossRef](#)] [[PubMed](#)]

16. Feng, J.; Sun, Q.; Li, Z.; Sun, Z.; Jia, K. Back-Propagation Neural Network-Based Reconstruction Algorithm for Diffuse Optical Tomography. *J. Biomed. Opt.* **2018**, *24*, 051407. [[CrossRef](#)]
17. Wang, X.; Xuan, Z.; Zhu, X.; Sun, H.; Li, J.; Xie, Z. Near-Infrared Photoresponsive Drug Delivery Nanosystems for Cancer Photo-Chemotherapy. *J. Nanobiotechnology* **2020**, *18*, 108. [[CrossRef](#)] [[PubMed](#)]
18. Zhu, B.; Sevick-Muraca, E.M. A Review of Performance of Near-Infrared Fluorescence Imaging Devices Used in Clinical Studies. *Br. J. Radiol.* **2015**, *88*, 20140547. [[CrossRef](#)] [[PubMed](#)]
19. Xu, W.; Wang, D.; Tang, B.Z. NIR-II AIEgens: A Win–Win Integration towards Bioapplications. *Angew. Chemie-Int. Ed.* **2021**, *60*, 7476–7487. [[CrossRef](#)]
20. Dai, H.; Wang, X.; Shao, J.; Wang, W.; Mou, X.; Dong, X. NIR-II Organic Nanotheranostics for Precision Oncotherapy. *Small* **2021**, *17*, 2102646. [[CrossRef](#)]
21. Lei, Z.; Zhang, F. Molecular Engineering of NIR-II Fluorophores for Improved Biomedical Detection. *Angew. Chemie-Int. Ed.* **2021**, *60*, 16294–16308. [[CrossRef](#)] [[PubMed](#)]
22. Furusawa, A.; Okada, R.; Inagaki, F.; Wakiyama, H.; Kato, T.; Furumoto, H.; Fukushima, H.; Okuyama, S.; Choyke, P.L.; Kobayashi, H. CD29 Targeted Near-Infrared Photoimmunotherapy (NIR-PIT) in the Treatment of a Pigmented Melanoma Model. *Oncoimmunology* **2022**, *11*, 2019922. [[CrossRef](#)] [[PubMed](#)]
23. Kobayashi, H.; Furusawa, A.; Rosenberg, A.; Choyke, P.L. Near-Infrared Photoimmunotherapy of Cancer: A New Approach That Kills Cancer Cells and Enhances Anti-Cancer Host Immunity. *Int. Immunol.* **2021**, *33*, 7–15. [[CrossRef](#)]
24. Kato, T.; Wakiyama, H.; Furusawa, A.; Choyke, P.L.; Kobayashi, H. Near Infrared Photoimmunotherapy; a Review of Targets for Cancer Therapy. *Cancers* **2021**, *13*, 2535. [[CrossRef](#)] [[PubMed](#)]
25. Kobayashi, H.; Choyke, P.L. Near-Infrared Photoimmunotherapy of Cancer. *Acc. Chem. Res.* **2019**, *52*, 2332–2339. [[CrossRef](#)] [[PubMed](#)]
26. Maruoka, Y.; Wakiyama, H.; Choyke, P.L.; Kobayashi, H. Near Infrared Photoimmunotherapy for Cancers: A Translational Perspective. *EBioMedicine* **2021**, *70*, 103501. [[CrossRef](#)]
27. Tang, L.; Li, J.; Zhao, Q.; Pan, T.; Zhong, H.; Wang, W. Advanced and Innovative Nano-Systems for Anticancer Targeted Drug Delivery. *Pharmaceutics* **2021**, *13*, 1151. [[CrossRef](#)] [[PubMed](#)]
28. Moramkar, N.; Bhatt, P. Insight into Chitosan Derived Nanotherapeutics for Anticancer Drug Delivery and Imaging. *Eur. Polym. J.* **2021**, *154*, 110540. [[CrossRef](#)]
29. Scutigliani, E.M.; Liang, Y.; Crezee, H.; Kanaar, R.; Krawczyk, P.M. Modulating the Heat Stress Response to Improve Hyperthermia-Based Anticancer Treatments. *Cancers* **2021**, *13*, 1243. [[CrossRef](#)] [[PubMed](#)]
30. Anani, T.; Rahmati, S.; Sultana, N.; David, A.E. MRI-Traceable Theranostic Nanoparticles for Targeted Cancer Treatment. *Theranostics* **2020**, *11*, 579–601. [[CrossRef](#)] [[PubMed](#)]
31. Bahman, F.; Pittalà, V.; Haider, M.; Greish, K. Enhanced Anticancer Activity of Nanoformulation of Dasatinib against Triple-Negative Breast Cancer. *J. Pers. Med.* **2021**, *11*, 559. [[CrossRef](#)] [[PubMed](#)]
32. Ding, J.; Lu, G.; Nie, W.; Huang, L.L.; Zhang, Y.; Fan, W.; Wu, G.; Liu, H.; Xie, H.Y. Self-Activatable Photo-Extracellular Vesicle for Synergistic Trimodal Anticancer Therapy. *Adv. Mater.* **2021**, *33*, 2005562. [[CrossRef](#)]
33. Li, Y.; Zhou, R.; Xiao, D.; Shi, S.; Peng, S.; Wu, S.; Wu, P.; Lin, Y. Polypeptide Uploaded Efficient Nanophotosensitizers to Overcome Photodynamic Resistance for Enhanced Anticancer Therapy. *Chem. Eng. J.* **2021**, *403*, 126344. [[CrossRef](#)]
34. Mouratidis, P.X.E.; Costa, M.; Rivens, I.; Repasky, E.E.; Ter Haar, G. Pulsed Focused Ultrasound Can Improve the Anti-Cancer Effects of Immune Checkpoint Inhibitors in Murine Pancreatic Cancer. *J. R. Soc. Interface* **2021**, *18*, 20210266. [[CrossRef](#)]
35. Fishell, A.K.; Arbeláez, A.M.; Valdés, C.P.; Burns-Yocum, T.M.; Sherafati, A.; Richter, E.J.; Torres, M.; Eggebrecht, A.T.; Smyser, C.D.; Culver, J.P. Portable, Field-Based Neuroimaging Using High-Density Diffuse Optical Tomography. *Neuroimage* **2020**, *215*, 116541. [[CrossRef](#)]
36. Applegate, M.B.; Karrobi, K.; Angelo, J.P.; Austin, W.M.; Tabassum, S.M.; Aguénounon, E.; Tilbury, K.; Saager, R.B.; Gioux, S.; Roblyer, D.M. OpenSFDI: An Open-Source Guide for Constructing a Spatial Frequency Domain Imaging System. *J. Biomed. Opt.* **2020**, *25*, 016002. [[CrossRef](#)]
37. Burley, T.A.; Maczyńska, J.; Shah, A.; Szopa, W.; Harrington, K.J.; Boulton, J.K.R.; Mrozek-Wilczkiewicz, A.; Vinci, M.; Bamber, J.C.; Kaspera, W.; et al. Near-Infrared Photoimmunotherapy Targeting EGFR-Shedding New Light on Glioblastoma Treatment. *Int. J. Cancer* **2018**, *142*, 2363–2374. [[CrossRef](#)] [[PubMed](#)]
38. Sherafati, A.; Snyder, A.Z.; Eggebrecht, A.T.; Bergonzi, K.M.; Burns-Yocum, T.M.; Lugar, H.M.; Ferradal, S.L.; Robichaux-Viehoever, A.; Smyser, C.D.; Palanca, B.J.; et al. Global Motion Detection and Censoring in High-Density Diffuse Optical Tomography. *Hum. Brain Mapp.* **2020**, *41*, 4093–4112. [[CrossRef](#)]
39. Angelo, J.P.; Chen, S.-J.K.; Ochoa, M.; Sunar, U.; Gioux, S.; Intes, X. Review of Structured Light in Diffuse Optical Imaging. *J. Biomed. Opt.* **2018**, *24*, 071602. [[CrossRef](#)]
40. Qi, H.; Zhao, F.Z.; Ren, Y.T.; Qiao, Y.B.; Wei, L.Y.; Islam, M.A.; Ruan, L.M. Experimental Research on Noninvasive Reconstruction of Optical Parameter Fields Based on Transient Radiative Transfer Equation for Diagnosis Applications. *J. Quant. Spectrosc. Radiat. Transf.* **2019**, *222–223*, 1–11. [[CrossRef](#)]
41. Chen, L.Y.; Yu, J.M.; Pan, M.C.; Sun, S.Y.; Chou, C.C.; Pan, M.C. Comparisons of Diffuse Optical Imaging between Direct-Current and Amplitude-Modulation Instrumentations. *Opt. Quantum Electron.* **2016**, *48*, 139. [[CrossRef](#)]

42. Cochran, J.M.; Busch, D.R.; Lin, L.; Minkoff, D.L.; Schweiger, M.; Arridge, S.; Yodh, A.G. Hybrid Time-Domain and Continuous-Wave Diffuse Optical Tomography Instrument with Concurrent, Clinical Magnetic Resonance Imaging for Breast Cancer Imaging. *J. Biomed. Opt.* **2019**, *24*, 051409. [[CrossRef](#)] [[PubMed](#)]
43. Yu, J.M.; Pan, M.C.; Chen, L.Y.; Pan, M.C.; Hsu, Y.F. Phantom Verification for a Ring-Scanning and Prone Diffuse Optical Imaging System. *Opt. Commun.* **2017**, *405*, 177–184. [[CrossRef](#)]
44. Oshina, I.; Spigulis, J. Beer–Lambert Law for Optical Tissue Diagnostics: Current State of the Art and the Main Limitations. *J. Biomed. Opt.* **2021**, *26*, 100901. [[CrossRef](#)] [[PubMed](#)]
45. Tan, C.W.; Zhang, P.P.; Zhou, X.X.; Wang, Z.X.; Xu, Z.Q.; Mao, W.; Li, W.X.; Huo, Z.Y.; Guo, W.S.; Yun, F. Quantitative Monitoring of Leaf Area Index in Wheat of Different Plant Types by Integrating NDVI and Beer-Lambert Law. *Sci. Rep.* **2020**, *10*, 929. [[CrossRef](#)]
46. Mallet, A.; Tsenkova, R.; Muncan, J.; Charnier, C.; Latriille, É.; Bendoula, R.; Steyer, J.P.; Roger, J.M. Relating Near-Infrared Light Path-Length Modifications to the Water Content of Scattering Media in Near-Infrared Spectroscopy: Toward a New Bouguer-Beer-Lambert Law. *Anal. Chem.* **2021**, *93*, 6817–6823. [[CrossRef](#)] [[PubMed](#)]
47. Ren, W.; Jiang, J.; Di Costanzo Mata, A.; Kalyanov, A.; Ripoll, J.; Lindner, S.; Charbon, E.; Zhang, C.; Rudin, M.; Wolf, M. Multimodal Imaging Combining Time-Domain near-Infrared Optical Tomography and Continuous-Wave Fluorescence Molecular Tomography. *Opt. Express* **2020**, *28*, 9860. [[CrossRef](#)]
48. Lighter, D.; Hughes, J.; Styles, I.; Filer, A.; Dehghani, H. Multispectral, Non-Contact Diffuse Optical Tomography of Healthy Human Finger Joints. *Biomed. Opt. Express* **2018**, *9*, 1445. [[CrossRef](#)]
49. Pera, V.; Karrobi, K.; Tabassum, S.; Teng, F.; Roblyer, D. Frequency Selection with Optical Property Uncertainty Estimates for Spatial Frequency Domain Imaging. *Opt. InfoBase Conf. Pap.* **2018**, Part F91-T, 1349–1357. [[CrossRef](#)]
50. Zhao, Y.; Applegate, M.B.; Istfan, R.; Pande, A.; Roblyer, D. Quantitative Real-Time Pulse Oximetry with Ultrafast Frequency-Domain Diffuse Optics and Deep Neural Network Processing. *Biomed. Opt. Express* **2018**, *9*, 5997. [[CrossRef](#)]
51. Mozumder, M.; Tarvainen, T. Time-Domain Diffuse Optical Tomography Utilizing Truncated Fourier Series Approximation. *J. Opt. Soc. Am. A* **2020**, *37*, 182. [[CrossRef](#)]
52. Mozumder, M.; Tarvainen, T. Evaluation of Temporal Moments and Fourier Transformed Data in Time-Domain Diffuse Optical Tomography. *J. Opt. Soc. Am. A* **2020**, *37*, 1845. [[CrossRef](#)]
53. Dalla Mora, A.; Di Sieno, L.; Behera, A.; Taroni, P.; Contini, D.; Torricelli, A.; Pifferi, A. The SiPM Revolution in Time-Domain Diffuse Optics. *Nucl. Instrum. Methods Phys. Res. Sect. A Accel. Spectrometers Detect. Assoc. Equip.* **2020**, *978*, 164411. [[CrossRef](#)]
54. Mitsunaga, M.; Ogawa, M.; Kosaka, N.; Rosenblum, L.T.; Choyke, P.L.; Kobayashi, H. Cancer Cell–Selective in Vivo near Infrared Photoimmunotherapy Targeting Specific Membrane Molecules. *Nat. Med.* **2011**, *17*, 1685–1691. [[CrossRef](#)] [[PubMed](#)]
55. Kessel, D. Photodynamic Therapy: A Brief History. *J. Clin. Med.* **2019**, *8*, 1581. [[CrossRef](#)]
56. Niu, N.; Zhou, H.; Liu, N.; Jiang, H.; Hussain, E.; Hu, Z.; Yu, C. A Smart Perylene Derived Photosensitizer for Lysosome-Targeted and Self-Assessed Photodynamic Therapy. *Chem. Commun.* **2019**, *55*, 1036–1039. [[CrossRef](#)] [[PubMed](#)]
57. Hussain, E.; Zhou, H.; Yang, N.; Shahzad, S.A.; Yu, C. Synthesis of Regioisomerically Pure Piperidine Substituted Perylenebisimide NIR Dyes: A Comparative Study of Spectroscopic, Electrochemical and Crystalline Properties. *Dye. Pigment.* **2017**, *147*, 211–224. [[CrossRef](#)]
58. Intes, X.; Chance, B. Multi-Frequency Diffuse Optical Tomography. *J. Mod. Opt.* **2005**, *52*, 2139–2159. [[CrossRef](#)]
59. Chen, C.; Kavuri, V.C.; Wang, X.; Li, R.; Liu, H.; Huang, J. Multi-Frequency Diffuse Optical Tomography for Cancer Detection. In Proceedings of the 2015 IEEE 12th International Symposium on Biomedical Imaging (ISBI), Brooklyn Bridge, NY, USA, 16–19 April 2015; pp. 67–70.
60. Applegate, M.B.; Gómez, C.A.; Roblyer, D.M. Modulation Frequency Selection and Efficient Look-up Table Inversion for Frequency Domain Diffuse Optical Spectroscopy. *J. Biomed. Opt.* **2021**, *26*, 036007. [[CrossRef](#)]
61. Hsu, Y.Y.; Gan, H.W.; Lee, B.T.; Hsu, Y.F.; Jiang, H.; Pan, M.C. Diffuse Optical Imaging through Simultaneous Multiple-Sinusoids Driving Light Sources. *Opt. InfoBase Conf. Pap.* **2020**, *2020*, 4–5. [[CrossRef](#)]
62. Fan, W.; Eggebrecht, A.T. Effect of Modulation Frequency on Image Quality in Frequency Domain High-Density Diffuse Optical Tomography in Infant Head. *Opt. InfoBase Conf. Pap.* **2022**, *8*, 1–19. [[CrossRef](#)]
63. Wang, H.; Xia, F.; Han, G.; Zhao, Z.; Chen, H.; Wang, J. Optical Parameters Detection with Multi-Frequency Modulation Based on NIR DPDW. *Infrared Phys. Technol.* **2019**, *97*, 135–141. [[CrossRef](#)]
64. Eklund, M.; Jäderling, F.; Discacciati, A.; Bergman, M.; Annerstedt, M.; Aly, M.; Glaessgen, A.; Carlsson, S.; Grönberg, H.; Nordström, T. MRI-Targeted or Standard Biopsy in Prostate Cancer Screening. *N. Engl. J. Med.* **2021**, *385*, 908–920. [[CrossRef](#)]
65. Ntziachristos, V.; Yodh, A.G.; Schnall, M.D.; Chance, B. MRI-Guided Diffuse Optical Spectroscopy of Malignant and Benign Breast Lesions. *Neoplasia* **2002**, *4*, 347–354. [[CrossRef](#)] [[PubMed](#)]
66. Vavadi, H.; Mostafa, A.; Zhou, F.; Uddin, K.M.S.; Althobaiti, M.; Xu, C.; Bansal, R.; Ademuyiwa, F.; Poplack, S.; Zhu, Q. Compact Ultrasound-Guided Diffuse Optical Tomography System for Breast Cancer Imaging. *J. Biomed. Opt.* **2018**, *24*, 021203. [[CrossRef](#)] [[PubMed](#)]
67. Xu, C.; Vavadi, H.; Merkulov, A.; Li, H.; Erfanzadeh, M.; Mostafa, A.; Gong, Y.; Salehi, H.; Tannenbaum, S.; Zhu, Q. Ultrasound-Guided Diffuse Optical Tomography for Predicting and Monitoring Neoadjuvant Chemotherapy of Breast Cancers. *Ultrason. Imaging* **2016**, *38*, 5–18. [[CrossRef](#)] [[PubMed](#)]

68. Sarmanova, O.E.; Burikov, S.A.; Dolenko, S.A.; Isaev, I.V.; Laptinskiy, K.A.; Prabhakar, N.; Karaman, D.Ş.; Rosenholm, J.M.; Shenderova, O.A.; Dolenko, T.A. A Method for Optical Imaging and Monitoring of the Excretion of Fluorescent Nanocomposites from the Body Using Artificial Neural Networks. *Nanomed. Nanotechnol. Biol. Med.* **2018**, *14*, 1371–1380. [[CrossRef](#)]
69. Jolivot, R.; Vabres, P.; Marzani, F. Reconstruction of Hyperspectral Cutaneous Data from an Artificial Neural Network-Based Multispectral Imaging System. *Comput. Med. Imaging Graph.* **2011**, *35*, 85–88. [[CrossRef](#)]
70. Zhang, M.; Zou, Y.; Li, S.; Zhu, Q. Auto Encoder Based Deep Learning Reconstruction for Diffuse Optical Tomography. *Opt. InfoBase Conf. Pap.* **2022**, 3–4. [[CrossRef](#)]
71. Balasubramaniam, G.M.; Wiesel, B.; Biton, N.; Kumar, R.; Kupferman, J.; Arnon, S. Tutorial on the Use of Deep Learning in Diffuse Optical Tomography. *Electronics* **2022**, *11*, 305. [[CrossRef](#)]
72. Smith, J.T.; Ochoa, M.; Faulkner, D.; Haskins, G.; Intes, X. Deep Learning in Macroscopic Diffuse Optical Imaging. *J. Biomed. Opt.* **2022**, *27*, 020901. [[CrossRef](#)]
73. Ben Yedder, H.; BenTaieb, A.; Shokoufi, M.; Zahiremami, A.; Golnaraghi, F.; Hamarneh, G. Deep Learning Based Image Reconstruction for Diffuse Optical Tomography. In *Lecture Notes in Computer Science (Including Subseries Lecture Notes in Artificial Intelligence and Lecture Notes in Bioinformatics)*; Springer: Cham, Sweden, 2018; Volume 11074 LNCS, pp. 112–119, ISBN 9783030001285.
74. Yao, B.; Li, W.; Pan, W.; Yang, Z.; Chen, D.; Li, J.; Qu, J. Image Reconstruction with a Deep Convolutional Neural Network in High-Density Super-Resolution Microscopy. *Opt. Express* **2020**, *28*, 15432. [[CrossRef](#)] [[PubMed](#)]
75. Sabir, S.; Cho, S.; Kim, Y.; Pua, R.; Heo, D.; Kim, K.H.; Choi, Y.; Cho, S. Convolutional Neural Network-Based Approach to Estimate Bulk Optical Properties in Diffuse Optical Tomography. *Appl. Opt.* **2020**, *59*, 1461. [[CrossRef](#)] [[PubMed](#)]
76. Xu, Q.; Wang, X.; Jiang, H. Convolutional Neural Network for Breast Cancer Diagnosis Using Diffuse Optical Tomography. *Vis. Comput. Ind. Biomed. Art* **2019**, *2*, 1–6. [[CrossRef](#)]
77. Lv, Y.; Li, F.; Wang, S.; Lu, G.; Bao, W.; Wang, Y.; Tian, Z.; Wei, W.; Ma, G. Near-Infrared Light-Triggered Platelet Arsenal for Combined Photothermal-Immunotherapy against Cancer. *Sci. Adv.* **2021**, *7*, eabd7614. [[CrossRef](#)]
78. Nagaya, T.; Nakamura, Y.; Sato, K.; Zhang, Y.F.; Ni, M.; Choyke, P.L.; Ho, M.; Kobayashi, H. Near Infrared Photoimmunotherapy with an Anti-Mesothelin Antibody. *Oncotarget* **2016**, *7*, 23361–23369. [[CrossRef](#)] [[PubMed](#)]
79. Sato, K.; Nagaya, T.; Nakamura, Y.; Harada, T.; Choyke, P.L.; Kobayashi, H. Near Infrared Photoimmunotherapy Prevents Lung Cancer Metastases in a Murine Model. *Oncotarget* **2015**, *6*, 19747–19758. [[CrossRef](#)] [[PubMed](#)]
80. Nagaya, T.; Friedman, J.; Maruoka, Y.; Ogata, F.; Okuyama, S.; Clavijo, P.E.; Choyke, P.L.; Allen, C.; Kobayashi, H. Host Immunity Following Near-Infrared Photoimmunotherapy Is Enhanced with PD-1 Checkpoint Blockade to Eradicate Established Antigenic Tumors. *Cancer Immunol. Res.* **2019**, *7*, 401–413. [[CrossRef](#)] [[PubMed](#)]
81. Sato, K.; Nagaya, T.; Choyke, P.L.; Kobayashi, H. Near Infrared Photoimmunotherapy in the Treatment of Pleural Disseminated NSCLC: Preclinical Experience. *Theranostics* **2015**, *5*, 698–709. [[CrossRef](#)] [[PubMed](#)]
82. Nagaya, T.; Sato, K.; Harada, T.; Nakamura, Y.; Choyke, P.L.; Kobayashi, H. Near Infrared Photoimmunotherapy Targeting EGFR Positive Triple Negative Breast Cancer: Optimizing the Conjugate-Light Regimen. *PLoS ONE* **2015**, *10*, e0136829. [[CrossRef](#)] [[PubMed](#)]
83. Isobe, Y.; Sato, K.; Nishinaga, Y.; Takahashi, K.; Taki, S.; Yasui, H.; Shimizu, M.; Endo, R.; Koike, C.; Kuramoto, N.; et al. Near Infrared Photoimmunotherapy Targeting DLL3 for Small Cell Lung Cancer. *EBioMedicine* **2020**, *52*, 102632. [[CrossRef](#)]
84. Nagaya, T.; Nakamura, Y.; Okuyama, S.; Ogata, F.; Maruoka, Y.; Choyke, P.L.; Kobayashi, H. Near-Infrared Photoimmunotherapy Targeting Prostate Cancer with Prostate-Specific Membrane Antigen (PSMA) Antibody. *Mol. Cancer Res.* **2017**, *15*, 1153–1162. [[CrossRef](#)]
85. Ogawa, M.; Tomita, Y.; Nakamura, Y.; Lee, M.J.; Lee, S.; Tomita, S.; Nagaya, T.; Sato, K.; Yamauchi, T.; Iwai, H.; et al. Immunogenic Cancer Cell Death Selectively Induced by near Infrared Photoimmunotherapy Initiates Host Tumor Immunity. *Oncotarget* **2017**, *8*, 10425–10436. [[CrossRef](#)]
86. Shirasu, N.; Yamada, H.; Shibaguchi, H.; Kuroki, M.; Kuroki, M. Potent and Specific Antitumor Effect of CEA-Targeted Photoimmunotherapy. *Int. J. Cancer* **2014**, *135*, 2697–2710. [[CrossRef](#)]
87. Sano, K.; Nakajima, T.; Choyke, P.L.; Kobayashi, H. The Effect of Photoimmunotherapy Followed by Liposomal Daunorubicin in a Mixed Tumor Model: A Demonstration of the Super-Enhanced Permeability and Retention Effect after Photoimmunotherapy. *Mol. Cancer Ther.* **2014**, *13*, 426–432. [[CrossRef](#)]
88. Sato, K.; Choyke, P.L.; Kobayashi, H. Photoimmunotherapy of Gastric Cancer Peritoneal Carcinomatosis in a Mouse Model. *PLoS ONE* **2014**, *9*, e113276. [[CrossRef](#)]
89. Hanaoka, H.; Nagaya, T.; Sato, K.; Nakamura, Y.; Watanabe, R.; Harada, T.; Gao, W.; Feng, M.; Phung, Y.; Kim, I.; et al. Glypican-3 Targeted Human Heavy Chain Antibody as a Drug Carrier for Hepatocellular Carcinoma Therapy. *Mol. Pharm.* **2015**, *12*, 2151–2157. [[CrossRef](#)]
90. Sato, K.; Hanaoka, H.; Watanabe, R.; Nakajima, T.; Choyke, P.L.; Kobayashi, H. Near Infrared Photoimmunotherapy in the Treatment of Disseminated Peritoneal Ovarian Cancer. *Mol. Cancer Ther.* **2015**, *14*, 141–150. [[CrossRef](#)]
91. Jing, H.; Weidensteiner, C.; Reichardt, W.; Gaedicke, S.; Zhu, X.; Grosu, A.L.; Kobayashi, H.; Niedermann, G. Imaging and Selective Elimination of Glioblastoma Stem Cells with Theranostic Near-Infrared-Labeled CD133-Specific Antibodies. *Theranostics* **2016**, *6*, 862–874. [[CrossRef](#)]
92. Nagaya, T.; Nakamura, Y.; Sato, K.; Harada, T.; Choyke, P.L.; Kobayashi, H. Near Infrared Photoimmunotherapy of B-Cell Lymphoma. *Mol. Oncol.* **2016**, *10*, 1404–1414. [[CrossRef](#)]

93. Railkar, R.; Krane, L.S.; Li, Q.Q.; Sanford, T.; Siddiqui, M.R.; Haines, D.; Vourganti, S.; Brancato, S.J.; Choyke, P.L.; Kobayashi, H.; et al. Epidermal Growth Factor Receptor (EGFR)-Targeted Photoimmunotherapy (PIT) for the Treatment of EGFR-Expressing Bladder Cancer. *Mol. Cancer Ther.* **2017**, *16*, 2201–2214. [[CrossRef](#)] [[PubMed](#)]
94. Nagaya, T.; Nakamura, Y.; Sato, K.; Harada, T.; Choyke, P.L.; Hodge, J.W.; Schlom, J.; Kobayashi, H. Near Infrared Photoimmunotherapy with Avelumab, an Anti-Programmed Death-Ligand 1 (PD-L1) Antibody. *Oncotarget* **2017**, *8*, 8807–8817. [[CrossRef](#)] [[PubMed](#)]
95. Nagaya, T.; Nakamura, Y.; Okuyama, S.; Ogata, F.; Maruoka, Y.; Choyke, P.L.; Allen, C.; Kobayashi, H. Syngeneic Mouse Models of Oral Cancer Are Effectively Targeted by Anti-CD44-Based NIR-PIT. *Mol. Cancer Res.* **2017**, *15*, 1667–1677. [[CrossRef](#)] [[PubMed](#)]
96. Siddiqui, M.R.; Railkar, R.; Sanford, T.; Crooks, D.R.; Eckhaus, M.A.; Haines, D.; Choyke, P.L.; Kobayashi, H.; Agarwal, P.K. Targeting Epidermal Growth Factor Receptor (EGFR) and Human Epidermal Growth Factor Receptor 2 (HER2) Expressing Bladder Cancer Using Combination Photoimmunotherapy (PIT). *Sci. Rep.* **2019**, *9*, 2084. [[CrossRef](#)] [[PubMed](#)]
97. Kiss, B.; van den Berg, N.S.; Ertsey, R.; McKenna, K.; Mach, K.E.; Zhang, C.A.; Volkmer, J.-P.; Weissman, I.L.; Rosenthal, E.L.; Liao, J.C. CD47-Targeted Near-Infrared Photoimmunotherapy for Human Bladder Cancer. *Clin. Cancer Res.* **2019**, *25*, 3561–3571. [[CrossRef](#)] [[PubMed](#)]
98. Lütje, S.; Heskamp, S.; Franssen, G.M.; Frielink, C.; Kip, A.; Hekman, M.; Fracasso, G.; Colombatti, M.; Herrmann, K.; Boerman, O.C.; et al. Development and Characterization of a Theranostic Multimodal Anti-PSMA Targeting Agent for Imaging, Surgical Guidance, and Targeted Photodynamic Therapy of PSMA-Expressing Tumors. *Theranostics* **2019**, *9*, 2924–2938. [[CrossRef](#)]
99. Watanabe, S.; Noma, K.; Ohara, T.; Kashima, H.; Sato, H.; Kato, T.; Urano, S.; Katsube, R.; Hashimoto, Y.; Tazawa, H.; et al. Photoimmunotherapy for Cancer-Associated Fibroblasts Targeting Fibroblast Activation Protein in Human Esophageal Squamous Cell Carcinoma. *Cancer Biol. Ther.* **2019**, *20*, 1234–1248. [[CrossRef](#)] [[PubMed](#)]
100. Wei, W.; Jiang, D.; Ehlerding, E.B.; Barnhart, T.E.; Yang, Y.; Engle, J.W.; Luo, Q.Y.; Huang, P.; Cai, W. CD146-Targeted Multimodal Image-Guided Photoimmunotherapy of Melanoma. *Adv. Sci.* **2019**, *6*, 1801237. [[CrossRef](#)] [[PubMed](#)]
101. Nagaya, T.; Okuyama, S.; Ogata, F.; Maruoka, Y.; Choyke, P.L.; Kobayashi, H. Near Infrared Photoimmunotherapy Using a Fiber Optic Diffuser for Treating Peritoneal Gastric Cancer Dissemination. *Gastric Cancer* **2019**, *22*, 463–472. [[CrossRef](#)] [[PubMed](#)]
102. Nakamura, Y.A.; Okuyama, S.; Furusawa, A.; Nagaya, T.; Fujimura, D.; Okada, R.; Maruoka, Y.; Eclarinal, P.C.; Choyke, P.L.; Kobayashi, H. Near-Infrared Photoimmunotherapy through Bone. *Cancer Sci.* **2019**, *110*, 3689–3694. [[CrossRef](#)] [[PubMed](#)]
103. Maruoka, Y.; Furusawa, A.; Okada, R.; Inagaki, F.; Fujimura, D.; Wakiyama, H.; Kato, T.; Nagaya, T.; Choyke, P.L.; Kobayashi, H. Combined CD44- And CD25-Targeted near-Infrared Photoimmunotherapy Selectively Kills Cancer and Regulatory T Cells in Syngeneic Mouse Cancer Models. *Cancer Immunol. Res.* **2020**, *8*, 345–355. [[CrossRef](#)]
104. Katsube, R.; Noma, K.; Ohara, T.; Nishiwaki, N.; Kobayashi, T.; Komoto, S.; Sato, H.; Kashima, H.; Kato, T.; Kikuchi, S.; et al. Fibroblast Activation Protein Targeted near Infrared Photoimmunotherapy (NIR PIT) Overcomes Therapeutic Resistance in Human Esophageal Cancer. *Sci. Rep.* **2021**, *11*, 1693. [[CrossRef](#)] [[PubMed](#)]
105. Okada, R.; Kato, T.; Furusawa, A.; Inagaki, F.; Wakiyama, H.; Choyke, P.L.; Kobayashi, H. Local Depletion of Immune Checkpoint Ligand CTLA4 Expressing Cells in Tumor Beds Enhances Antitumor Host Immunity. *Adv. Ther.* **2021**, *4*, 2000269. [[CrossRef](#)] [[PubMed](#)]
106. Mu, W.; Chu, Q.; Liu, Y.; Zhang, N. A Review on Nano-Based Drug Delivery System for Cancer Chemoimmunotherapy. *Nano-Micro Lett.* **2020**, *12*, 142. [[CrossRef](#)]
107. Kang, H.; Kang, M.W.; Kashiwagi, S.; Choi, H.S. NIR Fluorescence Imaging and Treatment for Cancer Immunotherapy. *J. Immunother.* **2022**, *10*, e004936. [[CrossRef](#)] [[PubMed](#)]
108. Ayana, G.; Ryu, J. Ultrasound-Responsive Nanocarriers for Breast Cancer Chemotherapy. *Micromachines* **2022**, *13*, 1508. [[CrossRef](#)] [[PubMed](#)]
109. Wang, Y.; Wang, Y.; Chen, G.; Li, Y.; Xu, W.; Gong, S. Quantum-Dot-Based Theranostic Micelles Conjugated with an Anti-EGFR Nanobody for Triple-Negative Breast Cancer Therapy. *ACS Appl. Mater. Interfaces* **2017**, *9*, 30297–30305. [[CrossRef](#)] [[PubMed](#)]
110. Asha Krishnan, M.; Yadav, K.; Roach, P.; Chelvam, V. A Targeted Near-Infrared Nanoprobe for Deep-Tissue Penetration and Imaging of Prostate Cancer. *Biomater. Sci.* **2021**, *9*, 2295–2312. [[CrossRef](#)] [[PubMed](#)]
111. Choi, H.; Choe, S.W. Acoustic Stimulation by Shunt-Diode Pre-Linearizer Using Very High Frequency Piezoelectric Transducer for Cancer Therapeutics. *Sensors* **2019**, *19*, 357. [[CrossRef](#)]
112. Cho, K.; Seo, J.; Heo, G.; Choe, S. An Alternative Approach to Detecting Cancer Cells by Multi-Directional Fluorescence Detection System Using Cost-Effective LED and Photodiode. *Sensors* **2019**, *19*, 2301. [[CrossRef](#)] [[PubMed](#)]
113. Choi, H.; Ryu, J.M.; Choe, S. woon A Novel Therapeutic Instrument Using an Ultrasound-Light-Emitting Diode with an Adjustable Telephoto Lens for Suppression of Tumor Cell Proliferation. *Meas. J. Int. Meas. Confed.* **2019**, *147*, 106865. [[CrossRef](#)]
114. Choi, H.; Choe, S.W.; Ryu, J.M. A Macro Lens-Based Optical System Design for Phototherapeutic Instrumentation. *Sensors* **2019**, *19*, 5427. [[CrossRef](#)] [[PubMed](#)]
115. Mudeng, V.; Nisa, W.; Sukmananda Suprpto, S. Computational Image Reconstruction for Multi-Frequency Diffuse Optical Tomography. *J. King Saud Univ.-Comput. Inf. Sci.* **2022**, *34*, 3527–3538. [[CrossRef](#)]